



Chinese Pharmaceutical Association  
Institute of Materia Medica, Chinese Academy of Medical Sciences

Acta Pharmaceutica Sinica B

[www.elsevier.com/locate/apsb](http://www.elsevier.com/locate/apsb)  
[www.sciencedirect.com](http://www.sciencedirect.com)



ORIGINAL ARTICLE

# The lysine methyltransferase SMYD2 facilitates neointimal hyperplasia by regulating the HDAC3–SRF axis

Xiaoxuan Zhong<sup>a,†</sup>, Xiang Wei<sup>a,b,†</sup>, Yan Xu<sup>c</sup>, Xuehai Zhu<sup>a,b</sup>, Bo Huo<sup>a</sup>,  
Xian Guo<sup>a</sup>, Gaoke Feng<sup>d</sup>, Zihao Zhang<sup>a</sup>, Xin Feng<sup>a</sup>, Zemin Fang<sup>a</sup>,  
Yuxuan Luo<sup>c,\*</sup>, Xin Yi<sup>d,\*</sup>, Ding-Sheng Jiang<sup>a,b,\*</sup>

<sup>a</sup>Division of Cardiovascular Surgery, Tongji Hospital, Tongji Medical College, Huazhong University of Science and Technology, Wuhan 430030, China

<sup>b</sup>Key Laboratory of Organ Transplantation, Ministry of Education, NHC Key Laboratory of Organ Transplantation, Chinese Academy of Medical Sciences, Wuhan 430030, China

<sup>c</sup>School of Life Science and Technology, Key Laboratory of Developmental Genes and Human Disease, Southeast University, Nanjing 210096, China

<sup>d</sup>Department of Cardiology, Renmin Hospital of Wuhan University, Wuhan 430060, China

Received 8 May 2023; received in revised form 21 September 2023; accepted 24 October 2023

## KEY WORDS

Neointima formation;  
Histone methylation;  
Histone acetylation;  
SRF acetylation;  
SMYD2;  
HDAC3;  
LLY-507;  
RGFP966

**Abstract** Coronary restenosis is an important cause of poor long-term prognosis in patients with coronary heart disease. Here, we show that lysine methyltransferase SMYD2 expression in the nucleus is significantly elevated in serum- and PDGF-BB-induced vascular smooth muscle cells (VSMCs), and in tissues of carotid artery injury-induced neointimal hyperplasia. *Smyd2* overexpression in VSMCs (*Smyd2*-vTg) facilitates, but treatment with its specific inhibitor LLY-507 or SMYD2 knockdown significantly inhibits VSMC phenotypic switching and carotid artery injury-induced neointima formation in mice. Transcriptome sequencing revealed that SMYD2 knockdown represses the expression of serum response factor (SRF) target genes and that SRF overexpression largely reverses the inhibitory effect of SMYD2 knockdown on VSMC proliferation. HDAC3 directly interacts with and deacetylates SRF, which enhances SRF transcriptional activity in VSMCs. Moreover, SMYD2 promotes HDAC3 expression *via* tri-methylation of H3K36 at its promoter. RGFP966, a specific inhibitor of HDAC3, not only counteracts the pro-proliferation effect of SMYD2 overexpression on VSMCs, but also inhibits carotid artery injury-induced neointima formation in mice. HDAC3 partially abolishes the inhibitory effect of SMYD2

\*Corresponding authors. Tel./fax: +86 27 69378454 (Dingsheng Jiang).

E-mail addresses: [jds@hust.edu.cn](mailto:jds@hust.edu.cn) (Ding-Sheng Jiang), [yixin2022@whu.edu.cn](mailto:yixin2022@whu.edu.cn) (Xin Yi), [yuxuanluo@seu.edu.cn](mailto:yuxuanluo@seu.edu.cn) (Yuxuan Luo).

<sup>†</sup>These authors made equal contributions to this work.

Peer review under the responsibility of Chinese Pharmaceutical Association and Institute of Materia Medica, Chinese Academy of Medical Sciences.

<https://doi.org/10.1016/j.apsb.2023.11.012>

2211-3835 © 2024 The Authors. Published by Elsevier B.V. on behalf of Chinese Pharmaceutical Association and Institute of Materia Medica, Chinese Academy of Medical Sciences. This is an open access article under the CC BY-NC-ND license (<http://creativecommons.org/licenses/by-nc-nd/4.0/>).



knockdown on VSMC proliferation in a deacetylase activity-dependent manner. Our results reveal that the SMYD2-HDAC3-SRF axis constitutes a novel and critical epigenetic mechanism that regulates VSMC phenotypic switching and neointimal hyperplasia.

© 2024 The Authors. Published by Elsevier B.V. on behalf of Chinese Pharmaceutical Association and Institute of Materia Medica, Chinese Academy of Medical Sciences. This is an open access article under the CC BY-NC-ND license (<http://creativecommons.org/licenses/by-nc-nd/4.0/>).

## 1. Introduction

Coronary artery disease is a major health concern globally and is associated with increasing economic burdens. Coronary artery stenosis is the main cause of myocardial ischemia. Percutaneous coronary intervention (PCI), balloon angioplasty, and coronary artery bypass grafting (CABG) are the most common revascularization treatment strategies for stenotic atherosclerotic lesions<sup>1</sup>. Although these procedures are effective, they result in vascular injury inducing abnormal proliferation of vascular smooth muscle cells (VSMCs), leading to restenosis or reocclusion affecting long-term arterial patency<sup>2,3</sup>. Anti-proliferative reagents that antagonize intimal VSMC proliferation have been considered potentially effective treatments for pathological neointima formation<sup>4,5</sup>. Drug-eluting stents, drug-coated balloons and arterial grafts have been used to reduce restenosis<sup>6</sup>, but better treatment options are needed to achieve better outcomes.

Aberrant VSMC proliferation, migration, and phenotypic switching are pivotal to intimal hyperplasia<sup>2,7</sup>. Serum response factor (SRF), a transcription factor binding to CArG box DNA sequences in gene promoters, is one of the most important regulators in controlling both the differentiation and proliferation of VSMCs by recruiting distinct accessory proteins<sup>8</sup>. Histone modifications, including methylation, are crucial for the regulation of chromatin spatial structure, and the looseness of chromatin determines whether transcription factors can effectively bind to DNA and initiate transcription<sup>9</sup>. Recent evidence has demonstrated a role for histone methylation (*e.g.*, H3K4me2) and acetylation (*e.g.*, H3K9/14ac) in controlling the chromatin-binding activity of SRF and its partners by affecting chromatin organization<sup>10,11</sup>. However, only a handful of studies have attempted to make connections between these regulatory layers in controlling the VSMC phenotype<sup>8</sup>. More work regarding interconnections between the SRF–CArG interaction, SRF cofactors, and histone modifications within CArG box sequences is needed.

Our previous studies have shown that inhibitors of either enhancer of zeste homolog 2 (EZH2) or euchromatic histone lysine methyltransferase 2 (EHMT2) inhibit VSMC growth and survival by activating autophagy<sup>12,13</sup>, which indicates that histone methylation potentially contributes to VSMC proliferation and neointima formation. Targeting the enzymes that mediate histone modifications, such as methyltransferases and acetylases, has gradually become a novel promising strategy for the treatment of disease<sup>14</sup>. The results of several clinical trials have demonstrated that some inhibitors of histone methyltransferases and deacetylases have preliminarily shown clinical activity, for example, tazemetostat (an inhibitor of EZH2), pinometostat (an inhibitor of disrupter of telomeric silencing 1-like (DOT1L)) and CHR-3996 (an inhibitor of class I histone deacetylases) have antitumor activity in humans<sup>15–17</sup>. However, whether targeting

histone methylation or acetylation can alleviate neointima formation remains largely unknown.

SET (Suppressor of variegation, Enhancer of Zeste, Trithorax) and MYND (Myeloid-Nervy-DEAF1) domain-containing protein 2 (SMYD2), a histone methyltransferase acting on both histone and nonhistone proteins, was shown to play a potential role in vascular remodeling<sup>12,18–20</sup>. A meta-analysis of genome-wide association studies showed that 1q32.3 (SMYD2) is a risk locus for abdominal aortic aneurysm (AAA)<sup>13,19</sup>. Furthermore, the SMYD2 promoter was hypomethylated in VSMCs taken from the aortic tissues of AAA patients compared with controls, and SMYD2 was downregulated in the arteries of AAA patients<sup>15,20</sup>. However, the role and mechanism of SMYD2 in VSMC proliferation and neointima formation remain unknown.

In the present study, we demonstrated that knockdown of SMYD2 arrests VSMCs in G0/G1 phase to inhibit their proliferation, while SMYD2 overexpression promotes the proliferation of VSMCs to accelerate vascular injury-induced neointima formation. The SMYD2 expression level in the nucleus is significantly increased in proliferating VSMCs, which promotes the expression of histone deacetylase 3 (HDAC3) *via* trimethylation of H3K36 (H3K36me3). HDAC3 directly interacts with and deacetylates SRF, enhancing the transcriptional activity of SRF to facilitate cyclin-dependent kinase 4 (CDK4) and CDK6 expression. Furthermore, the SMYD2 inhibitor LLY-507 and HDAC3 inhibitor RGFP966 markedly reduce carotid artery injury-induced neointima formation *in vivo*. Our results indicated that targeting SMYD2 or HDAC3 has great potential to reduce restenosis induced by balloon injury, PCI or CABG.

## 2. Materials and methods

### 2.1. Animal experiments

All experiments involving animals in this study were approved by the Animal Care and Use Committee of Tongji Hospital, Tongji Medical College, Huazhong University of Science and Technology. Mice were housed in a specific pathogen-free (SPF) animal facility with free access to food and water and on a 12-h light–dark cycle. Male C57BL/6J mice were purchased from GemPharmatech Co., Ltd., and the *Sm22α-creERT2* mice were obtained from Shanghai Model Organisms Center, Inc. To generate smooth muscle cell (SMC)-specific *Smyd2* transgenic (TG) mice, the transgene vector pCAG-CAT-*Smyd2* (mouse), which contains a CAG gene promoter-loxP-CAT gene-polyA-loxP-*Smyd2* gene-polyA, was microinjected into fertilized zygotes of C57BL/6J mice to obtain founder mice. The founder mice were identified by PCR amplification of tail DNA using a forward primer 5'-CATGTCTGGATCGATCCCCG-3' and a reverse primer 5'-CCCTTGCTCCATACCACCCC-3'. Exogenous *Smyd2*-positive

mice were crossed with *Sm22 $\alpha$ -creERT2* mice to obtain the *Smyd2-cTG* mice, which were injected with tamoxifen (30 mg/kg/day) for 5 consecutive days to induce the over-expression of SMYD2 (*Smyd2-vTG*) for subsequent experiments. The expression level of SMYD2 in the aortas of *Smyd2-vTG* mice was determined by immunohistochemistry.

The mouse model of neointima formation was generated as previously described<sup>2</sup>. Briefly, male mice (aged 9–10 weeks old, and weighed 24–26 g) were anesthetized by intraperitoneal injection of sodium pentobarbital (80 mg/kg). After that, the left carotid artery was carefully exposed through a midline neck incision. A transverse incision was made in the external carotid artery proximal to the suture after ligating the external carotid artery proximal to the bifurcation point and clipping the internal and common carotid arteries. Then, a guidewire (0.38 mm in diameter, no. C-SF-15-15; Cook, Bloomington, USA) was inserted through the incision into the arterial lumen toward the aortic arch and withdrawn five times with a rotating motion. Finally, the guidewire was removed, blood flow was restored, and the wound was sutured. Littermate control mice that underwent a similar procedure but without vascular injury served as the uninjured control mice. After surgery, intraperitoneal injections of LLY-507 (1 mg/kg/day) and RGFP966 (10 mg/kg/day) were used to treat the mice for 4 weeks. Dimethyl sulfoxide-treated mice served as the control mice.

## 2.2. Primary HASMC isolation, culture and treatments

Primary cultured human aortic smooth muscle cells (HASMCs) were isolated from the ascending aortas of heart transplant donors at Tongji Hospital, Tongji Medical College, Huazhong University of Science and Technology, China. The procedures involving human tissues were approved by the Review Board of Tongji Hospital, Tongji Medical College, Huazhong University of Science and Technology, Wuhan, China. The methods for the isolation and culture of primary HASMCs were similar to the protocol we previously reported<sup>21</sup>. Briefly, fresh aortic tissue was separated under a stereomicroscope to strip the intimal and residual adventitial tissues. Then, the aortic media were cut into 1–2 mm small pieces and spread evenly in culture flasks for 30 min. After the tissues firmly adhered to the wall of the culture flask, 5 mL of DMEM/F12 medium supplemented with 10% FBS (SH30084.03; HyClone) and 1% penicillin–streptomycin (15140-122; ThermoFisher Scientific) was added for cell culture. Spindle-shaped smooth muscle cells crawled out of the tissue block after the flask was left to stand for 5 days. The HASMCs were routinely passaged at a confluence of approximately 80% for the following experiments. To knock down or overexpress genes, we inserted the corresponding shRNA targeting sequence into the pLKO.1 vector or inserted the CDS of the gene into the *pHAGE* vector to generate knockdown or overexpression plasmids (the primers are listed in [Supporting Information Table S1](#)), respectively, and then packaged these plasmids into lentiviruses, including lenti-Flag, lenti-SMYD2(WT)-Flag, lenti-SMYD2(Y240A)-Flag, lenti-HA, lenti-HDAC3-HA, lenti-HDAC3(Y298H)-HA, lenti-SRF-Flag, lenti-shRNA, and lenti-shSMYD2 lentiviruses, to infect HASMCs at a multiplicity of infection (MOI) of 50. In addition, LLY-507 (2  $\mu$ mol/L, S7575, Selleck), RGFP966 (15  $\mu$ mol/L, S7229, Selleck) and PDGF-BB (10–20 ng/mL, 220-BB-010, R&D Systems) were used to treat HASMCs.

## 2.3. Protein extraction and Western blot analysis

Total protein was extracted from HASMCs by using RIPA lysis buffer, and Western blotting was performed as previously described<sup>21</sup>. For extraction of nuclear and cytoplasmic proteins, HASMCs treated with different concentrations of FBS or PDGF-BB were collected and washed with cold PBS and then lysed with cytoplasmic lysis buffer (20 mmol/L HEPES, 1 mmol/L EDTA, 10 mmol/L KCl, 2 mmol/L MgCl<sub>2</sub>, 0.25% NP40 and protease inhibitors) on ice for 30 min. The lysate was centrifuged at 5000  $\times$  g for 5 min at 4  $^{\circ}$ C. The supernatant was collected as the cytoplasmic lysate. Then, the precipitates were washed twice with cold PBS and resuspended in nuclear lysis buffer (20 mmol/L HEPES, 1 mmol/L EDTA, 420 mmol/L NaCl, 10 mmol/L KCl, 2 mmol/L MgCl<sub>2</sub>, 0.25% NP40, 25% glycerol and protease inhibitors) on ice for 10 min. The nuclear lysate was sonicated at 25% power 15 times at 30 s intervals on ice. The lysate was centrifuged at 14,000  $\times$  g for 5 min at 4  $^{\circ}$ C. The supernatant was collected as the nuclear lysate. The antibodies used in this study were as follows: the primary antibodies of SMYD2 (21290-1-AP) and LaminB1(12987-1-AP) were obtained from Proteintech Group; The primary antibody p-Histone H3 (Ser10) (p-H3, sc-8656-R) was obtained from SANTA CRUZ; anti-PCNA (GTX100539), anti-H3K27ac (GTX128944), anti-MMP2 (GTX634832) and anti-MMP9 (GTX100458) were purchased from Genetex; the antibodies of CDK4 (#12790), CDK6 (#3136), HDAC3 (#3949), SRF (#5147S), H3K4me2 (#9725), H3K4me3 (#9727), and H3K36me1 (#14111) were obtained from Cell Signaling Technology; the antibodies of Flag (F1804) and HA (H3663) were purchased from Sigma–Aldrich; the antibodies of H3K4me1 (ab8895), H3K36me2 (ab9049), and H3K36me3 (ab9050) were obtained from Abcam; and the anti-GAPDH (AC033) and anti- $\beta$ -actin (AC026) were from ABclonal Biotechnology.

## 2.4. Quantitative real-time PCR

Quantitative real-time PCR (qPCR) was performed to measure the mRNA levels of target genes. Total mRNA was isolated from cultured cells with TRIzol Reagent (AM9738; ThermoFisher Scientific). cDNA was synthesized *via* reverse transcription of RNA with a Transcriptor First Strand cDNA Synthesis Kit (AM9738; Thermo Fisher Scientific). qPCR was performed on a CFX96 Touch™ Real-Time PCR Detection System using SYBR Green PCR Master Mix (11201ES08, Yeasen) in accordance with the manufacturer's instructions. The relative expression levels of the target genes were calculated and normalized to the loading control 18S rRNA. All the primers used in this study are listed in [Supporting Information Table S2](#).

## 2.5. RNA sequencing and data analysis

HASMCs infected with lenti-shRNA or lenti-shSMYD2 were collected for RNA sequencing. RNA sequencing was performed by Novogene Co., Ltd. (Beijing, China) on the Illumina NovaSeq platform. After quantitative processing, the read counts were used to identify the differentially expressed genes (DEGs) with an adjusted *P* value  $\leq 0.05$  and fold change  $\geq 1.5$  with the DESeq2 package (version 1.32.0) in R software (version 4.1.1). The *P* values were corrected for multiple comparisons by Benjamini–Hochberg method. Functional enrichment analyses (GO, KEGG, and GSEA) were implemented with the clusterProfiler (version 4.0.5) R package based on the DEGs. The terms

with adjusted  $P$  values  $< 0.05$  were considered significantly enriched. To analyze the enrichment of SRF downstream target genes, we first downloaded the list of SRF downstream genes from the GeneCards database and then intersected it with the DEGs identified by RNA sequencing to obtain the downstream target genes regulated by SRF considered in this study.

## 2.6. Histological and immunohistochemical staining

Carotid arteries were harvested from mice with or without vascular injury surgery. Coronary arteries were collected from pigs with and without coronary stenting as previously described<sup>22</sup>. The arteries were fixed with 4% paraformaldehyde, followed by paraffin embedding. Then, the sections were stained with hematoxylin and eosin (H&E) to observe neointima formation. The intimal area and the ratio of the intimal/medial area (I/M) were determined using Image-Pro Plus software (Media Cybernetics) by a single observer who was blinded to the treatment protocols.

For immunohistochemical staining, after deparaffinization and rehydration, the arterial sections were subjected to a high-pressure antigen retrieval process. The sections were blocked for 60 min in 5% BSA diluted with PBS and then incubated with the appropriate primary antibody overnight at 4 °C. After being rewarmed at 37 °C for 1 h, the sections were washed with PBS and incubated with secondary antibodies for 1 h. The sections were stained with a diaminobenzene (DAB) horseradish peroxidase color development kit (ZLI-9017, ZSGB-BIO). The antibodies used for immunohistochemical staining in this study including anti-SMYD2 (21290-1-AP, Proteintech), anti-HDAC3 (#3949, Cell Signaling Technology) and anti-PCNA (GTX100539, GeneTex).

The localization and expression of SMYD2 were determined according to immunofluorescence staining method, after deparaffinization and rehydration, the arterial sections were subjected to a high-pressure antigen retrieval process. And then the slides were blocked with blocking buffer (5% bovine serum albumin) at 37 °C for 1 h, the primary antibody SMYD2 (21290-1-AP, Proteintech),  $\alpha$ -SMA (ab7817, Abcam), and SM22 $\alpha$  (ab14106, Abcam) were incubated for overnight at 4 °C. After being rewarmed at 37 °C for 1 h, the sections were washed with PBS and incubated with secondary antibodies (Alexa Fluor 568 donkey anti-Rabbit IgG [H + L; Thermo Fisher Scientific, A10042] for SMYD2 and SM22 $\alpha$ , and the Alexa Fluor 488 donkey anti-mouse IgG [H + L; Thermo Fisher Scientific, A21202] for  $\alpha$ -SMA) for 1 h at 37 °C and followed with diamidino-phenyl-indole (DAPI) staining in the dark. After washing with PBS, an Olympus light microscope BX53 system was applied for image capture.

## 2.7. Cell proliferation assays

The proliferation of HASMCs was assessed by cell counting, the cell counting kit-8 (CCK-8) method, a 5-ethynyl-2'-deoxyuridine (EdU) incorporation assay and immunofluorescence staining of Ki67 as previously described<sup>23</sup>. First, HASMCs stimulated as indicated were counted by using a Cellometer Mini (Nexcelom) at 0 h and 48 h to monitor their growth rate. Second, a CCK-8 kit (Cell Counting Kit-8, BS350A; Biosharp) was applied to evaluate cell viability and proliferation according to the manufacturer's instructions. The absorbance was measured at 450 nm using a Biotek Synergy HT microplate reader. Third, DNA synthesis was examined by an EdU incorporation assay with a Cell-Light™ EdU Apollo 567 In Vitro Kit (C10310-1, RiboBio) to evaluate HASMC proliferation. The EdU-positive cells were counted and

normalized to the total number of Hoechst 33342-stained cells. Finally, immunofluorescence staining of Ki67 (ab16667, Abcam), a proliferation marker, was performed to evaluate HASMC proliferation. The Ki67-positive cells were counted and normalized to the total number of cells with nuclear DAPI staining.

## 2.8. Transwell assay

The migration of HASMCs was assessed by Transwell assay, and the method was performed as previously described<sup>24</sup>. HASMCs were synchronized by serum starvation for 24 h and then resuspended in 0.5% FBS medium. The upper chamber was added with  $3 \times 10^4$  cells in 100  $\mu$ L medium. After the cells adhered for 2.5 h, a total of 800  $\mu$ L medium containing 10% FBS was added in the lower chamber. After 12 h, the membranes to which the cells migrated were fixed with 4% paraformaldehyde for 15 min and then stained with 0.1% crystal violet for 30 min. The membranes were washed with PBS and non-migrated cells were wiped gently with a cotton swab. Then, the cells were observed with a microscope.

## 2.9. Flow cytometry

HASMCs infected with lenti-shRNA or lenti-shSMYD2 were harvested and washed twice with PBS. The HASMCs were then collected by centrifugation for 10 min at 4 °C. After fixation with precooled 70% ethanol at -20 °C overnight, the HASMCs were washed twice with cold PBS, and 150  $\mu$ L of Ribonuclease A (R5125; Sigma-Aldrich) and 150  $\mu$ L of propidium iodide (PI; P4864; Sigma-Aldrich) solution (1.5  $\mu$ g of PI) were subsequently added to the cells and incubated at 4 °C in a dark room for 4 h. Then, the HASMCs were sorted by using a BD FACS Aria III cell sorter, and FlowJo software (version 10.7.2) was used for cell cycle analysis.

## 2.10. Luciferase reporter assay

The luciferase reporter plasmid pGL3-*HDAC3* was generated with primers 5'-TGCTAGCCCGGGCTCGAGTTTCTCCCACCCTGACCAC-3' (forward) and 5'-TACCGGAATGCCAAGCTTCATTAAGCAGAGGACGCCAC-3' (reverse). The pGL3-*SRE* luciferase reporter plasmid was generously donated by Dr. Jun Gong (Tongji Hospital, Tongji Medical College, Huazhong University of Science and Technology). For the luciferase assay, HEK293T cells were plated in 24-well plates and cultured for 12 h prior to transfection. The cells were cotransfected with 0.4  $\mu$ g of the shRNA, shSMYD2, Flag, HA, SMYD2(WT)-Flag, SMYD2(Y240A)-Flag, HDAC3(WT)-HA or HDAC3(Y298H)-HA plasmid and 0.1  $\mu$ g of the pGL3-*HDAC3* or pGL4-*SRE* plasmid as well as 0.01  $\mu$ g of the *Renilla* luciferase (TK) plasmid per well. After 48 h, the cells were lysed with 100  $\mu$ L of passive lysis buffer (E1910, Promega Corporation). After removing cell debris by centrifugation, we measured the relative luciferase activity as the ratio of firefly luciferase (pGL3-*HDAC3* or pGL4-*SRE*) to TK activity.

## 2.11. Coimmunoprecipitation (Co-IP)

HASMCs and HEK293T cells were lysed in immunoprecipitation buffer (20 mmol/L Tris-HCl (pH 7.4), 150 mmol/L NaCl, 1 mmol/L EDTA, and 1% Triton X-100) supplemented with protease inhibitors (HY-K0010, MCE). Approximately 1–3 mg of total

protein was incubated with 1  $\mu$ g of an anti-Flag antibody (Sigma–Aldrich, F1804), anti-HA antibody (Sigma–Aldrich, H3663) or IgG (Santa Cruz, sc2025), and protein A/G agarose beads (B23202, Biomake) were then added and incubated overnight at 4 °C. The beads were washed 5 times with wash buffer (0.5 mol/L NaCl in immunoprecipitation buffer). After that, proteins were eluted with SDS loading buffer and analyzed by Western blotting.

### 2.12. Chromatin immunoprecipitation (ChIP)-PCR

HASMCs were cross-linked with 1% formaldehyde for 10 min at room temperature, and glycine was then added to stop the cross-linking reaction. After centrifugation, the cell pellets were collected in cold cell lysis buffer and sonicated. The samples were subjected to immunoprecipitation with an anti-H3K36me3 antibody (Abcam, ab9045) or IgG (Santa Cruz, sc2025) and incubated with protein A/G magnetic beads (Biotool, B23202). After washing twice with low-salt wash buffer (2 mmol/L EDTA, 20 mmol/L Tris-HCl (pH 8.0), 0.1% SDS, 1% Triton X-100, and 150 mmol/L NaCl), once with high-salt wash buffer (2 mmol/L EDTA, 20 mmol/L Tris-HCl (pH 8.0), 0.1% SDS, 1% Triton X-100, and 500 mmol/L NaCl), once with LiCl wash buffer (1 mmol/L EDTA, 10 mmol/L Tris-HCl (pH 8.0), 250 mmol/L LiCl, 1% deoxycholic acid, 200 mmol/L NaCl, and 1% NP-40) and three times with TE buffer (1 mmol/L EDTA, 10 mmol/L Tris-HCl (pH 8.0)), the beads were resuspended in elution buffer (1% SDS, 0.1 mol/L NaHCO<sub>3</sub>) to elute the protein/DNA complexes. The eluates were reverse cross-linked by incubation with proteinase K and 5 mol/L NaCl at 65 °C overnight. DNA was recovered with a DNA purification kit (Beyotime, D0033) and analyzed by quantitative PCR using the following primer pairs: human *HDAC3*, 5'-TGGGACACGGAGGTTTTGAG-3' (forward) and 5'-ACCAGGCTATGGGTCAATGC-3' (reverse).

### 2.13. Statistical analysis

All data are presented as the means  $\pm$  standard deviation (SD). To evaluate the significance of differences in the data between two groups, Student's two-tailed *t*-test was used for analysis. For comparisons among more than two groups, one-way ANOVA was used, followed by the Bonferroni *post hoc* test for data with homogeneity of variance or Tamhane's T2 test for heteroscedastic data. The individual statistical tests and the sample size of each set of animals used for each experiment are indicated in the figure legends. A value of *P* < 0.05 was considered to be statistically significant. All statistical analyses were performed with SPSS software (version 23.0).

## 3. Results

### 3.1. SMYD2 expression is increased within the nucleus during VSMC proliferation

To determine whether SMYD2 participates in the proliferation of VSMCs, HASMCs were treated with different concentrations of serum and PDGF-BB to induce proliferation. As expected, the protein levels of the proliferation markers, proliferating cell nuclear antigen (PCNA) and phosphorylated histone H3 (p-H3) were increased by serum stimulation (Fig. 1A). The SMYD2 steady-state protein level was elevated in these proliferated HASMCs (Fig. 1A). Cellular fractionation revealed that SMYD2 remained

in the cytoplasmic fraction in serum-free treated HASMCs (Fig. 1B). However, the SMYD2 protein level was increased more than 2-fold in the nuclear fraction of serum-treated HASMCs, suggesting that SMYD2 expression is elevated in the nucleus but not in the cytoplasm following HASMC proliferation (Fig. 1B). To further validate above results, we treated HASMCs with PDGF-BB which is a common method for inducing VSMC proliferation and phenotypic switching<sup>25</sup>. Consistent with serum treatment, PDGF-BB treatment significantly elevated SMYD2 protein level in the nucleus of HASMCs (Fig. 1C and D). Furthermore, in a mouse model of carotid artery injury displaying neointima formation (Fig. 1E), increased SMYD2 abundance, especially in the nucleus, was detected in the VSMCs of injured arteries (Fig. 1F). Therefore, these results indicate that elevated SMYD2 expression within the nucleus may contribute to VSMC proliferation and neointima formation.

### 3.2. Inhibition of SMYD2 suppresses VSMC phenotypic switching and neointima formation

To test the potential therapeutic effect of SMYD2 inhibition on neointimal hyperplasia, we treated wild-type (WT) mice with LLY-507 (a specific inhibitor of SMYD2) for 28 days after vascular injury. LLY-507 strikingly inhibited the level of trimethylation of H3K36 (H3K36me3) which is a substrate of SMYD2 both in uninjured and injured arteries (Supporting Information Fig. S1A). Although LLY-507 had little effect on arteries under normal condition (Fig. S1B), it obviously suppressed the increase of the neointimal area in response to carotid artery injury (Fig. 2A–C). Compared with DMSO, the expression level of PCNA was suppressed, while the expression levels of  $\alpha$ -SMA and SM22 $\alpha$  were increased in vascular injury-induced mice treated with LLY-507 (Fig. S1C and S1D). To explore whether LLY-507 affects VSMC proliferation *in vitro*, HASMCs were treated with LLY-507 to inhibit SMYD2 activity and cell proliferation was evaluated. SMYD2 inhibition dramatically suppressed HASMC proliferation, as indicated by the reduced cell number, cell viability, and number of EdU- or Ki67-positive HASMCs (Fig. 2D, E and Fig. S1E).

To further determine whether SMYD2 is required for VSMC proliferation, we silenced SMYD2 in HASMCs by lentiviral transduction (Fig. 2F). SMYD2 knockdown significantly reduced the number and viability of HASMCs (Fig. 2G and H). SMYD2 silencing decreased the number of EdU- or Ki67-positive HASMCs (Fig. 2I–K), and inhibited the expression of cell proliferation markers PCNA and p-H3 (Fig. 2L). The results of flow cytometry showed that SMYD2 knockdown increased the number of G0/G1-phase HASMCs and decreased the number of S-phase HASMCs, suggesting that G1 arrest occurred in these cells (Fig. 2M). The expression of CDK4 and CDK6, two important regulators in the G1 check point of the cell cycle<sup>26</sup>, were obviously downregulated in HASMCs with *SMYD2* knockdown (Fig. 2N).

Given that VSMC proliferation is often accompanied by increased migration capacity<sup>27</sup>, we further detected the impact of SMYD2 on VSMC migration. The results of Transwell assays demonstrated that the migration of HASMCs was inhibited by SMYD2 knockdown (Fig. S1F). We subsequently detected the protein expression of matrix metalloproteinases (MMPs), which play a critical role in the process of VSMC migration<sup>28</sup>. Our results show that compared with lenti-shRNA, the expression levels of MMP2 and MMP9 were reduced in HASMCs with SMYD2

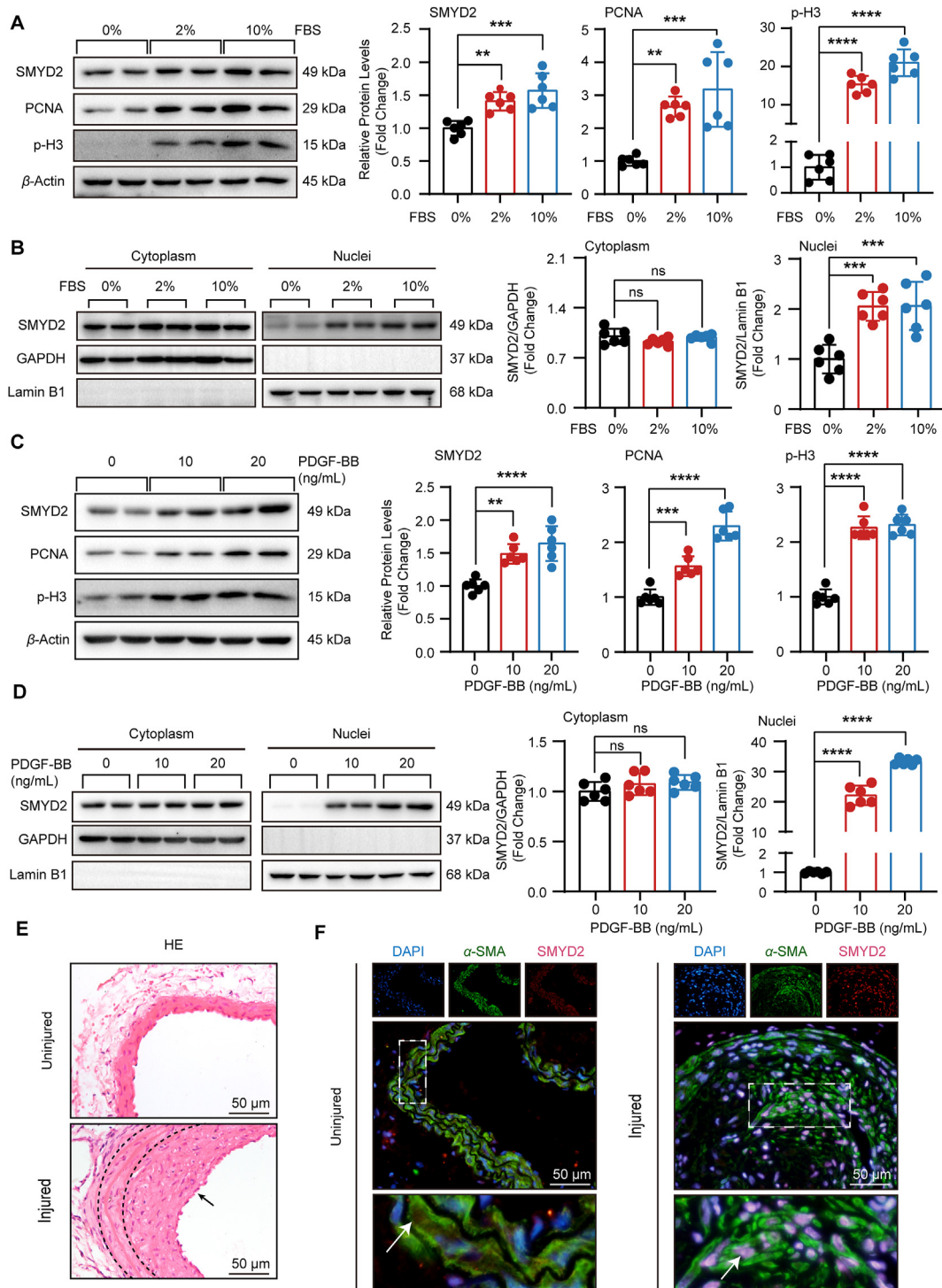


**Figure 1** SMYD2 expression is increased during VSMC proliferation. (A) Western blot analysis and quantification showing the protein levels of SMYD2, PCNA and p-H3 in HASMCs treated with different concentrations of FBS for 48 h ( $n = 6$ ). (B) SMYD2 protein levels in the cytoplasmic and nuclear fractions extracted from FBS-induced HASMCs ( $n = 6$ ). (C) Western blot analysis and quantification showing the protein levels of SMYD2, PCNA and p-H3 in HASMCs treated with different concentrations of PDGF-BB for 48 h ( $n = 6$ ). (D) SMYD2 protein levels in the cytoplasmic and nuclear fractions extracted from PDGF-BB treated HASMCs ( $n = 6$ ). (E) Representative images of hematoxylin and eosin (H&E) staining of intimal sections from uninjured and injured carotid arteries of mice ( $n = 6-8$ ). (F) Immunofluorescence staining of SMYD2 and  $\alpha$ -SMA in uninjured and injured carotid arteries ( $n = 3$ ). The data are presented as the mean  $\pm$  SD, ns indicates no significance; \*\* $P < 0.01$ ; \*\*\* $P < 0.001$ ; \*\*\*\* $P < 0.0001$ . SMYD2: histone methyltransferase SET and MYND domain containing 2; VSMC: vascular smooth muscle cell; HASMC: human aortic smooth muscle cell; PCNA: proliferating cell nuclear antigen; p-H3: phosphorylated histone H3; FBS: fetal bovine serum; GAPDH: glyceraldehyde 3-phosphate dehydrogenase; PDGF-BB: platelet-derived growth factor subunit B;  $\alpha$ -SMA: alpha-smooth muscle actin.

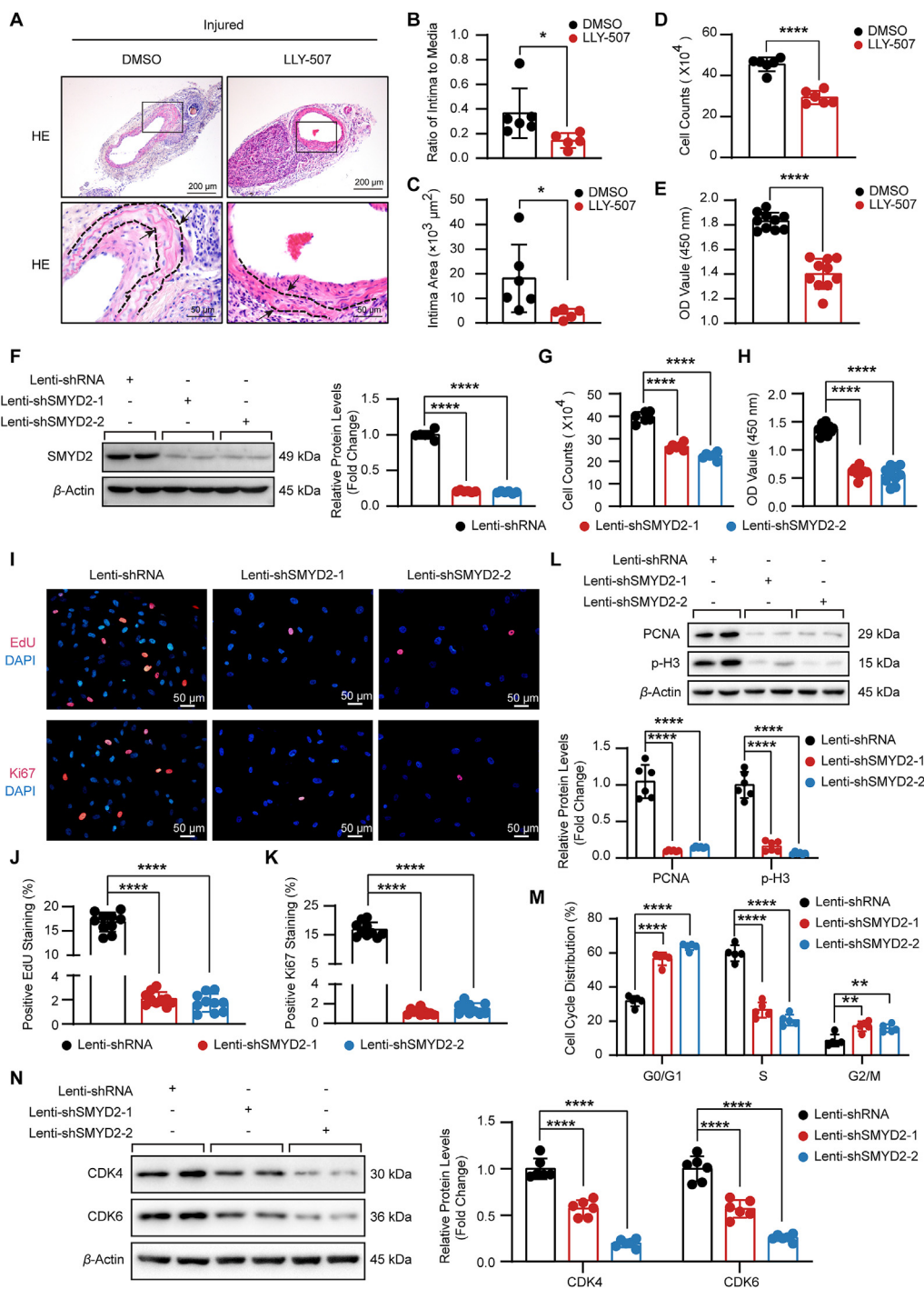


**Figure 2** SMYD2 is required for HASMC proliferation. (A) H&E staining of carotid arteries from mice treated with dimethyl sulfoxide (DMSO) or LLY-507 (1 mg/kg/day) for 28 days after carotid artery injury ( $n = 5-6$ ). (B) and (C) Quantification of the intimal/medial area ratio (B) and the intimal area (C) in the indicated groups ( $n = 5-6$ ). (D) The number of HASMCs treated with LLY-507 (2 μmol/L) for 48 h ( $n = 6$ ). (E) The proliferation of LLY-507-treated HASMCs was evaluated by a CCK8 assay ( $n = 10$ ). (F) SMYD2 was silenced with two different target sequences (shSMYD2-1 and shSMYD2-2) in HASMCs by lentiviral transduction ( $n = 6$ ). (G) The counts of HASMCs infected with lenti-shRNA or lenti-shSMYD2 ( $n = 6$ ). (H) HASMC proliferation after SMYD2 knockdown was evaluated by a CCK8 assay ( $n = 10$ ). (I) Representative images of immunofluorescence staining of 5-ethynyl-2'-deoxyuridine (EdU)-positive (top) and Ki67-positive (bottom) HASMCs after SMYD2 knockdown. (J) and (K) Quantification of EdU- (J) and Ki67-positive (K) HASMCs treated as described in I ( $n = 10$ ). (L) Western blot analysis and quantification showing the protein levels of PCNA and p-H3 in SMYD2-silenced HASMCs ( $n = 6$ ). (M) Cell cycle analysis of HASMCs by flow cytometry ( $n = 5$ ). (N) Western blot analysis and quantification showing the protein levels of CDK4 and CDK6 in SMYD2-silenced HASMCs ( $n = 6$ ). The data are presented as the mean  $\pm$  SD, \* $P < 0.05$ ; \*\*\*\* $P < 0.0001$ . CDK4: cyclin-dependent kinase 4; CDK6: cyclin-dependent kinase 6.

knockdown (Fig. S1G). Taken together, these results indicate that SMYD2 is essential for VSMC phenotypic switching and carotid artery injury-induced neointima formation.

### 3.3. VSMC-specific SMYD2 overexpression promotes neointima formation

To further test for a functional role of SMYD2 in neointima formation, we engineered inducible VSMC-specific *Smyd2* conditional transgenic (*Smyd2*-vTG) mice by mating CAG-Loxp-CAT-polyA-Loxp-*Smyd2*-polyA mice with *Sm22 $\alpha$ -creERT2* mice. Then, at 6 weeks of age, the *Smyd2*-cTG mice were injected with tamoxifen for 5 days to induce the overexpression of SMYD2 in VSMCs (*Smyd2*-vTG) (Supporting Information Fig. S2A). Two weeks after tamoxifen injection, SMYD2 protein overexpression in VSMCs was validated by using immunohistochemical staining (Fig. S2B). *Smyd2*-vTG mice were healthy and showed no apparent vascular morphological or pathological abnormalities under normal condition (Fig. S2C). After carotid artery injury, *Smyd2*-vTG mice showed an increased neointimal area compared with that in non-transgenic (NTG) mice (Fig. 3A–C). Carotid artery injury-induced protein expression of cell proliferation marker PCNA was significantly higher, while the expression levels of contractile markers  $\alpha$ -SMA and SM22 $\alpha$  were lower in *Smyd2*-vTG mice than in NTG mice (Fig. S2D and S2E). Together, these results indicate that SMYD2 overexpression accelerates carotid artery injury-induced neointima formation.

### 3.4. SMYD2 promotes VSMC proliferation in a methyltransferase activity-dependent manner

Next, we sought to evaluate whether SMYD2 is sufficient to induce VSMC proliferation and migration. We engineered a lentivirus express SMYD2 and infected HASMCs (Fig. 3D). Compared with the control group, SMYD2(WT) overexpression significantly increased the total HASMC number and viability (Fig. 3E and F). SMYD2(WT) overexpression increased the incorporation of EdU in HASMCs, suggesting the promotion of S-phase entry (Fig. 3G and H). Ki67 staining was also utilized to determine the proliferative activity of HASMCs. There were more Ki67-positive nuclei in SMYD2(WT)-overexpressed HASMCs than in control cells (Fig. 3G and I). Consistent with these findings, the expression of the cell proliferation markers PCNA and p-H3 was also enhanced by SMYD2(WT) overexpression (Fig. 3J). Moreover, SMYD2(WT) overexpression also accelerated the expression of CDK4 and CDK6, which are known to act in G1 phase (Fig. 3K). Because tyrosine 240 is crucial for the methyltransferase activity of SMYD2<sup>29</sup> and inhibition of SMYD2 activity by LLY-507 suppresses carotid artery injury-induced neointima formation, we engineered a mutant by substituting tyrosine 240 with alanine (Y240A) to explore whether methyltransferase activity is required for SMYD2-induced VSMC proliferation (Fig. 3D). Comparable numbers of HASMCs were found in the Y240A mutant and control groups (Fig. 3E and F). There was no difference in the number of EdU- and Ki67-positive nuclei between HASMCs expressing the Y240A construct and control HASMCs (Fig. 3G–I). The protein levels of PCNA, p-H3, CDK4, and CDK6 were not affected by SMYD2(Y240A) overexpression (Fig. 3J and K). Furthermore, the results of Transwell migration assays demonstrated that SMYD2(WT) but not SMYD2(Y240A) overexpression accelerated HASMC migration (Fig. S2F). Similarly, MMP2 and MMP9, the positive regulators of VSMC

migration, were upregulated by SMYD2(WT) overexpression in HASMCs, while comparable MMP2 and MMP9 protein levels were detected between SMYD2(Y240A) overexpressed HASMCs and lenti-Flag infected HASMCs (Supporting Information Fig. S2G). Taken together, these results suggest that SMYD2 overexpression promotes VSMC proliferation and migration in a manner dependent on its methyltransferase activity.

### 3.5. SRF is responsible for SMYD2-induced VSMC proliferation

To identify mechanisms leading to the inhibition of proliferation after SMYD2 silencing, we conducted RNA-seq analysis to identify transcriptomic changes in HASMCs. A total of 781 differentially expressed genes were identified, and the biological processes altered in SMYD2-silenced VSMCs including cell cycle, proliferation, differentiation and contraction (Fig. 4A and Supporting Information Fig. S3A–S3C). Interestingly, among these differentially expressed genes regulated by SMYD2, many are downstream target genes of SRF which is a critical transcription factor that regulates VSMC proliferation and differentiation<sup>30</sup> (Fig. 4B). Thus, we sought to determine whether SMYD2 regulates VSMC proliferation through SRF. SRF overexpression increased the protein levels of PCNA and p-H3 in SMYD2-silenced HASMCs (Fig. 4C). Furthermore, SRF overexpression rescued the SMYD2 knockdown-induced inhibition of HASMC proliferation, as indicated by the increased numbers of cells and EdU-positive nuclei (Fig. 4D–F). These results suggest that SRF is at least partially responsible for SMYD2-mediated VSMC proliferation.

To further determine the relationship between SMYD2 and SRF, we first tested whether SMYD2 regulates SRF expression in HASMCs. Unexpectedly, the expression of SRF was not affected by neither SMYD2 knockdown nor overexpression (Fig. S3D and S3E). SMYD2 often interacts with other proteins to regulate their activity and function<sup>18</sup>, while the results of co-IP assay showed that there was no interaction between SMYD2 and SRF (Fig. S3F and S3G). We further performed a reporter assay for the serum response element (SRE), the binding site of SRF. SMYD2 knockdown dramatically inhibited the binding activity of SRF to the SRE (Fig. S3H). Therefore, SMYD2 indirectly regulates SRF activity and at least one other molecule is involved in this process.

### 3.6. HDAC3 interacts with and deacetylates SRF to promote VSMC proliferation

It has been reported that SRF interacts with histone deacetylase 3 (HDAC3)<sup>31</sup>, a member of the family of class I HDACs, which regulate gene expression and protein activity by deacetylating histone and nonhistone proteins<sup>32</sup>. We confirmed the interaction between SRF and HDAC3 in HEK293T cells (Supporting Information Fig. S4A and S4B), and this interaction was also detected in HASMCs (Fig. 5A and B). To map the domain required for the interaction between SRF and HDAC3, truncation mutants of SRF or HDAC3 were expressed in HEK293T cells (Fig. 5C). We found that SRF bound to the 123–265 aa region of HDAC3 and that HDAC3 bound to the 301–508 aa region of SRF (Fig. 5D and E). Importantly, the binding of HDAC3 activated SRF in HASMCs, as HDAC3 increased SRE reporter activity, while the inactivating mutation of HDAC3 (HDAC3(Y298H)) has no obvious effect on SRF transcriptional activity (Fig. 5F). To test whether the deacetylase activity of HDAC3 is essential for SRF activation, RGFP966, a specific inhibitor of HDAC3, was used to

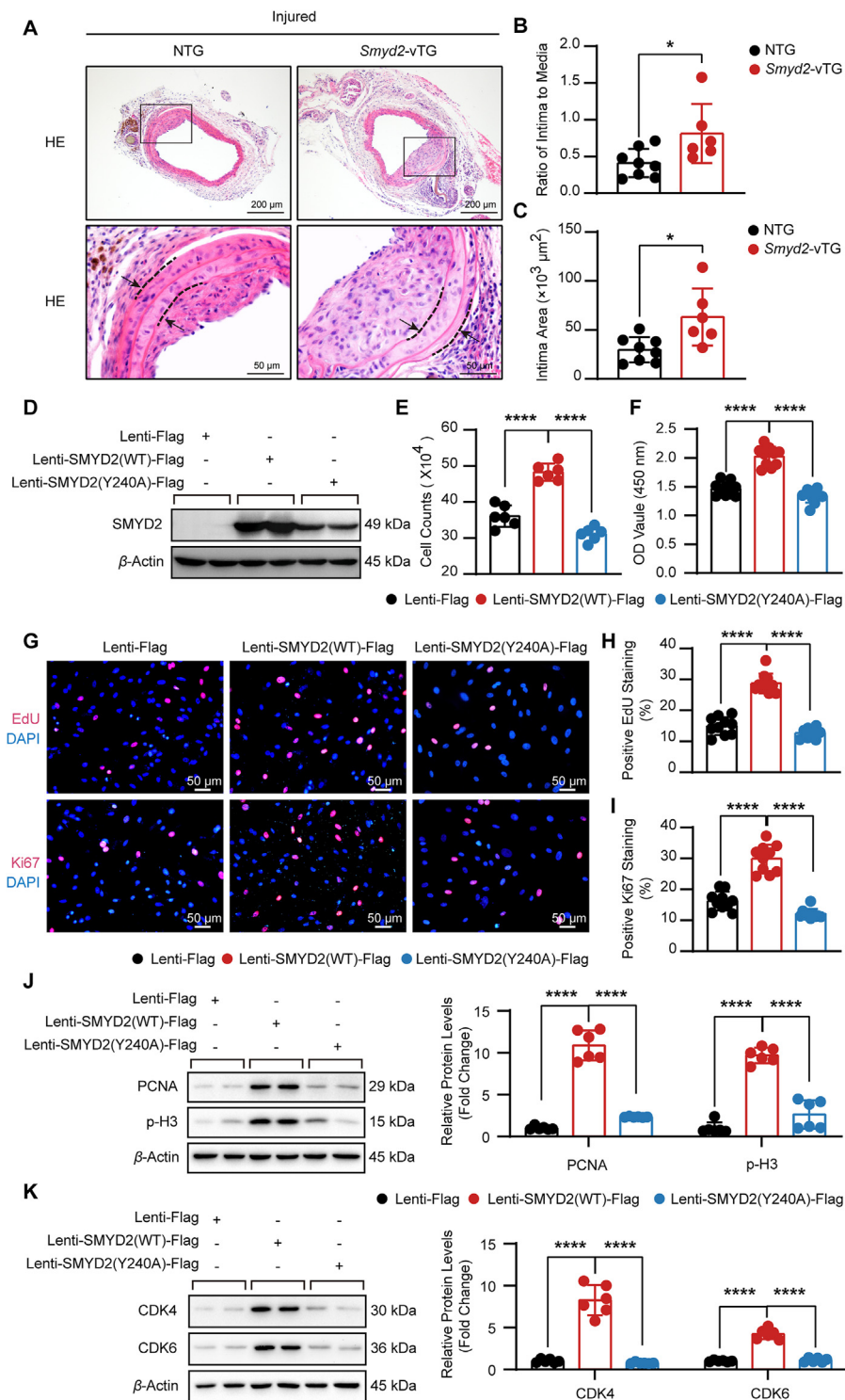


**Figure 3** VSMC-specific SMYD2 overexpression promotes carotid artery injury-induced neointima formation and VSMC proliferation. (A), Artery sections stained with H&E showing neointima formation in NTG and *Smyd2-vTG* mice 28 days after carotid artery injury ( $n = 6-8$ ). (B) and (C) Quantification of the intimal/media area ratio (B) and the intimal area (C) in the indicated groups ( $n = 6-8$ ). (D) SMYD2 expression in HASMCs infected with lentivirus expressing wild-type (WT) SMYD2 or mutated SMYD2 (tyrosine 240 to alanine, Y240A) was detected by using western blot ( $n = 6$ ). (E) The number of HASMCs infected with the indicated lentivirus ( $n = 6$ ). (F) HASMC proliferation after SMYD2 overexpression was evaluated by a CCK8 assay ( $n = 10$ ). (G) Representative images of immunofluorescence staining of EdU-positive (top) and Ki67-positive (bottom) HASMCs after SMYD2 overexpression. (H, I) Quantification of EdU-positive (H) and Ki67-positive (I) HASMCs treated as described in G ( $n = 10$ ). (J) Western blot analysis and quantification showing the protein levels of PCNA and p-H3 in SMYD2-overexpressing HASMCs ( $n = 6$ ). (K) The protein levels of CDK4 and CDK6 in SMYD2-overexpressing HASMCs ( $n = 6$ ). The data are presented as the mean  $\pm$  SD, \* $P < 0.05$ ; \*\*\*\* $P < 0.0001$ .

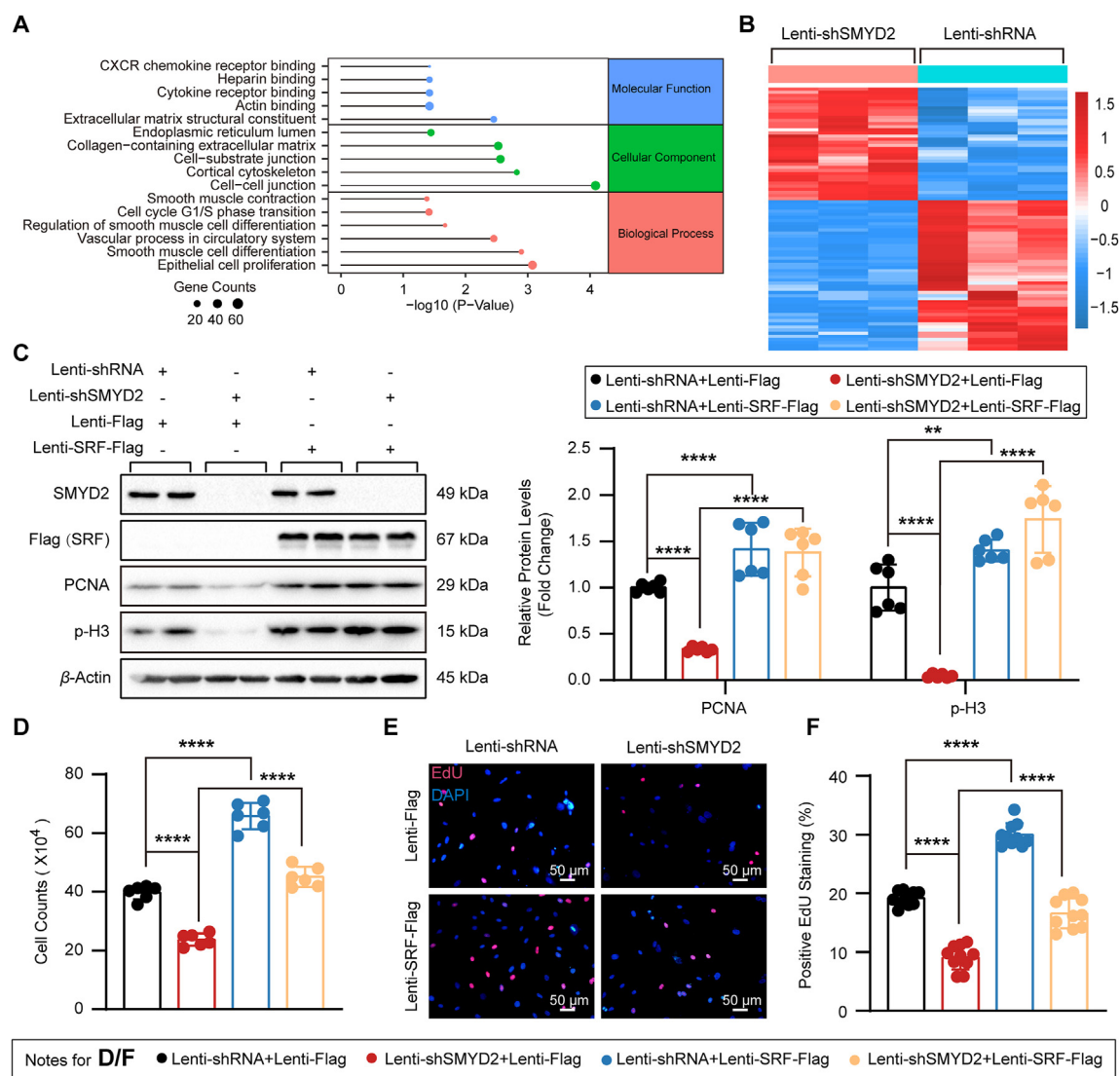


**Figure 4** SRF is responsible for SMYD2-induced VSMC proliferation. (A) Gene ontology analyses of the identified differentially expressed genes between control and SMYD2-silenced HASMCs ( $n = 3$ ). (B) Heatmap showing the differentially expressed SRF-targeted genes between control and SMYD2-silenced HASMCs ( $n = 3$ ). (C) Western blot analysis and quantification showing the protein levels of PCNA and p-H3 in SMYD2-silenced and/or SRF-overexpressing HASMCs ( $n = 6$ ). (D) The number of HASMCs treated as described in C ( $n = 6$ ). (E) and (F) Representative images of immunofluorescence staining (E) and quantification (F) of EdU-positive HASMCs in the indicated groups ( $n = 10$ ). The data are presented as the mean  $\pm$  SD,  $**P < 0.01$ ;  $****P < 0.0001$ . SRF: serum response factor.

treat cells. RGFP966 significantly decreased the transcriptional activity of SRF (Fig. 5G). Moreover, compared with DMSO control, the acetylation level of SRF was obviously elevated in HASMCs treated with RGFP966 (Fig. 5H). These results suggest that HDAC3 interacted with SRF and deacetylated SRF to enhance its transcriptional activity.

Next, we were curious about whether HDAC3 contributes to neointima formation *in vivo*. RGFP966 was used to treat mice with or without vascular injury. Compared with DMSO-treated mice, the level of H3K27ac, which was reported to be deacetylated by HDAC3<sup>33</sup>, was upregulated in carotid arteries of RGFP966-treated mice (Fig. S4C). Moreover, although in the uninjured group, RGFP966 had little effect on carotid arteries, mice with RGFP966 treatment showed thinner carotid artery injury-induced neointimal area than mice treated with DMSO (Fig. 5I–K, and Fig. S4D). *In vitro*, RGFP966 prominently inhibited HASMC proliferation, as

evidenced by the lower protein levels of PCNA and p-H3, the lower cell number, and the lower number of EdU-positive HASMCs than in the DMSO control group, and SRF overexpression largely abolished the inhibitory effect of RGFP966 on proliferation (Fig. S4E–S4H). These results indicate that HDAC3 physically and functionally interacts with SRF in VSMCs and that the deacetylase activity of HDAC3 is required for SRF-mediated VSMC proliferation.

### 3.7. SMYD2 induces HDAC3 expression by increasing H3K36me3 levels

The effect of HDAC3 on SRF led us to consider whether HDAC3 is regulated by SMYD2 to mediate the effect of SMYD2 on SRF. In our RNA-seq data, HDAC3 was found to be downregulated in SMYD2-silenced HASMCs (Supporting Information Fig. S5A),

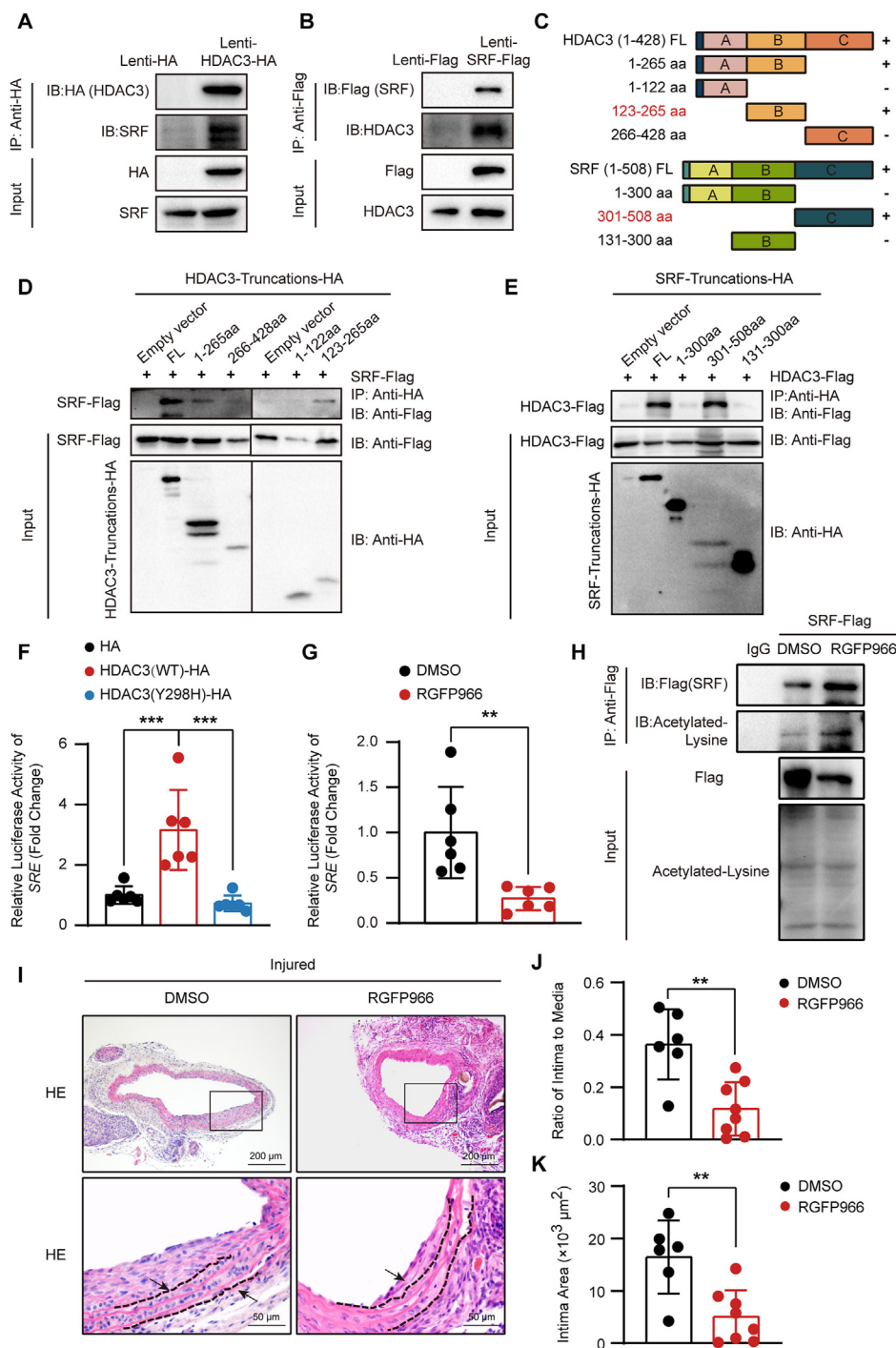


**Figure 5** HDAC3 interacts with, and deacetylates SRF to promote HASMC proliferation. (A, B) HDAC3 interacts with SRF. HASMCs were infected with lentiviruses expressing HDAC3-HA and SRF-Flag, and then anti-HA and anti-Flag antibodies were used for co-immunoprecipitation (co-IP) ( $n = 3$ ). (C) Schematic diagrams of the HDAC3 (top) and SRF (bottom) vectors used to map the SRF and HDAC3 binding domains. (D) Western blot analysis of HDAC3 deletion mutants or SRF after IP with lysates of HASMCs overexpressing the indicated vectors ( $n = 3$ ). (E) Western blot analysis of SRF deletion mutants or HDAC3 after IP with lysates of HASMCs overexpressing the indicated vectors ( $n = 3$ ). (F, G) Luciferase activity of the SRE in the HEK293T cells with indicated treatments ( $n = 6$ ). (H) The acetylation level of SRF was detected by using denatured IP; SRF was immunoprecipitated by using Flag antibody, and the acetylation level of SRF was detected by using pan-acetylated lysine antibody ( $n = 3$ ). (I) H&E staining of arteries from mice treated with dimethyl sulfoxide (DMSO) or RGFP966 (10 mg/kg/day) for 28 days after carotid artery injury ( $n = 6-8$ ). (J, K) Quantification of the intimal/medial area ratio (J) and the intimal area (K) in the indicated groups ( $n = 6-8$ ). The data are presented as the mean  $\pm$  SD, \*\* $P < 0.01$ ; \*\*\* $P < 0.001$ . HDAC3: histone deacetylase 3.

and the qPCR and Western blotting results further confirmed that SMYD2 silencing significantly decreased the *HDAC3* mRNA and protein levels in HASMCs (Fig. 6A and C), whereas SMYD2 overexpression increased *HDAC3* expression (Fig. 6B and D). However, overexpression of the SMYD2(Y240A) mutant did not

affect *HDAC3* expression (Fig. 6B and D), suggesting that the methyltransferase activity of SMYD2 is required for the induction of *HDAC3*. To confirm that *HDAC3* expression is regulated by SMYD2 *in vivo*, we evaluated the *HDAC3* level in WT mice treated with LLY-507 and in *Smyd2*-vTG mice by

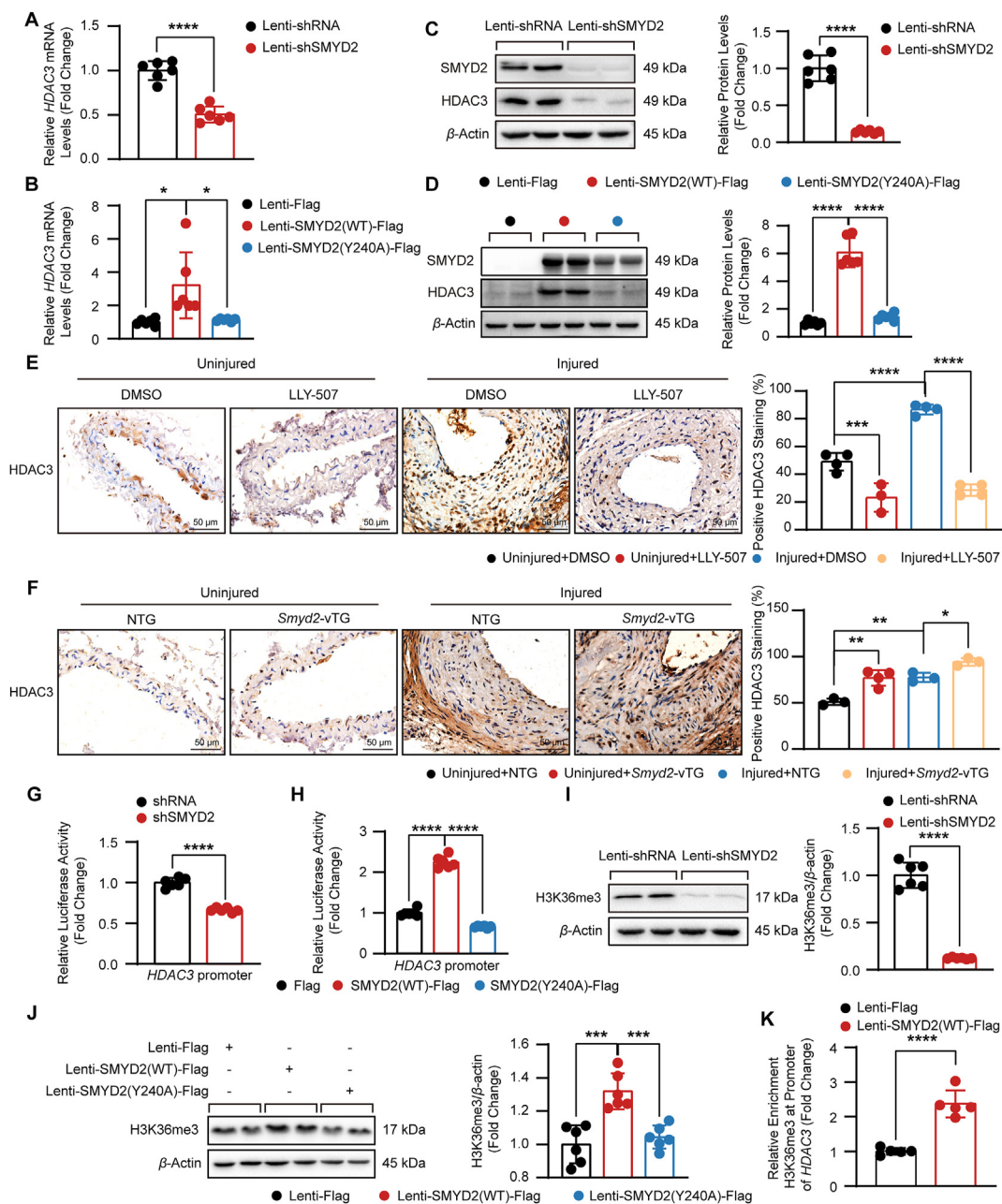


**Figure 6** SMYD2 induces *HDAC3* expression by increasing H3K36me3 levels. (A) *HDAC3* mRNA level in SMYD2-silenced HASMCs ( $n = 6$ ). (B) *HDAC3* mRNA level in SMYD2-overexpressing HASMCs ( $n = 6$ ). (C, D) Western blot analysis and quantification showing the *HDAC3* protein level in SMYD2-silenced (C) and SMYD2-overexpressing (D) HASMCs ( $n = 6$ ). (E) Immunohistochemical staining and quantitative data of *HDAC3* in the carotid arteries of DMSO- or LLY-507-treated mice with or without carotid artery injury surgery for 28 days ( $n = 3-4$ ). (F) Immunohistochemical staining and quantitative data of *HDAC3* in the carotid arteries of NTG and *Smyd2*-vTG mice with or without carotid artery injury surgery for 28 days ( $n = 3-4$ ). (G) Luciferase activity in HEK293T cells cotransfected with the PGL3-*HDAC3* reporter plasmid, SMYD2 knockdown plasmid and TK plasmid ( $n = 6$ ). (H) Luciferase activity in HEK293T cells cotransfected with the PGL3-*HDAC3* reporter plasmid along with the SMYD2 or mutated SMYD2 expression plasmid as well as the TK plasmid ( $n = 6$ ). (I, J) Western blot analysis and quantification showing the protein level of H3K36me3 in SMYD2-silenced (I) and SMYD2-overexpressing (J) HASMCs ( $n = 6$ ). (K) CHIP-PCR analysis was used to detect the enrichment of H3K36me3 at the *HDAC3* promoter in the HASMCs with or without SMYD2 overexpression ( $n = 5$ ). The data are presented as the mean  $\pm$  SD, \* $P < 0.05$ ; \*\* $P < 0.01$ ; \*\*\* $P < 0.001$ ; \*\*\*\* $P < 0.0001$ .

immunohistochemical staining. We found that compared with DMSO, inhibition of SMYD2 by LLY-507 reduced the HDAC3 level both in uninjured mice and in mice with carotid artery injury (Fig. 6E). A higher HDAC3 level was observed in the injured carotid arteries of *Smyd2*-vTG mice than that in NTG mice (Fig. 6F).

To further tease apart the relationship between SMYD2 and HDAC3, luciferase assays were performed by using a reporter construct harboring the *HDAC3* promoter. SMYD2 knockdown resulted in a decrease in *HDAC3* promoter activity, whereas SMYD2 overexpression induced an increase in reporter activity, a response that was abolished by the Y240A mutation (Fig. 6G and H). As the methyltransferase activity of SMYD2 is essential for HDAC3 induction and SMYD2 expression is significantly elevated in the nucleus during cell proliferation, we tested the methylation levels of H3K4 and H3K36, which are canonical substrates of SMYD2<sup>18</sup>, in SMYD2-silenced and SMYD2-overexpressing HASMCs. SMYD2 silencing decreased the levels of H3K36me3 by 88% and H3K4me2 by 40%, but did not affect the levels of H3K4me1/3 and H3K36me1/2 in HASMCs (Fig. 6I and Fig. S5B). Moreover, SMYD2 overexpression increased the level of H3K36me3, while the SMYD2(Y240A) mutation did not affect H3K36me3 level (Fig. 6J). Importantly, the enrichment of H3K36me3 at the *HDAC3* promoter was increased by SMYD2 overexpression (Fig. 6K). Taken together, these results suggest that SMYD2 controls HDAC3 expression by elevating the H3K36me3 level in the *HDAC3* promoter.

### 3.8. The deacetylase activity of HDAC3 is required for SMYD2-induced VSMC proliferation

To determine whether HDAC3 is the mediator of SMYD2-induced VSMC proliferation, we overexpressed HDAC3 in SMYD2-silenced HASMCs (Fig. 7A). HDAC3 overexpression promoted HASMC proliferation not only in the control group but also in the SMYD2-silenced group (Fig. 7A–C). To test the role of the deacetylase activity of HDAC3 in SMYD2-induced VSMC proliferation, we engineered a lentivirus expressing a mutant in which the catalytic tyrosine 298 residue was replaced with histidine (Y298H)<sup>34</sup>. The effect of the HDAC3(Y298H) mutant on HASMC proliferation was similar to that of the control (Fig. 7A–C). In addition, the HDAC3(Y298H) mutant did not alter the decrease in HASMC proliferation caused by SMYD2 silencing (Fig. 7A–C). To further support the hypothesis that HDAC3 activity is essential for SMYD2-induced VSMC proliferation, the HDAC3 inhibitor RGFP966 was used to treat HASMCs. Inhibition of HDAC3 by RGFP966 decreased the expression of proliferation markers and reduced the numbers of total HASMCs and proliferated HASMCs (Fig. 7D–F). Interestingly, SMYD2 overexpression failed to induce the cell proliferation of RGFP966-treated HASMCs (Fig. 7D–F). Taken together, these results indicate that the deacetylase activity of HDAC3 is required for SMYD2-induced VSMC proliferation.

### 3.9. Increased SMYD2 and HDAC3 expression in the coronary arteries in a porcine model of post-stent restenosis

Finally, we evaluated the relevance of these findings in a porcine model of post-stent restenosis, in which a vascular stent was installed to simulate stenting in clinical patients<sup>35</sup>. As expected, neointima formation was obviously observed six months after stenting, and the expression of PCNA was elevated in injured

vessels, suggesting that cell proliferation was activated (Fig. 8A). Consistent with our findings in mice, the protein abundances of SMYD2 and HDAC3 were significantly increased following vascular injury-induced neointima formation (Fig. 8A).

Collectively, our results demonstrate that under proliferative stimulations, the expression of SMYD2 is upregulated in the nucleus, which facilitates the expression of HDAC3 through trimethylation of H3K36. Subsequently, HDAC3 enhances the transcriptional activity of SRF by deacetylating it, thereby promoting the expression of proliferation-related genes (e.g., CDK4, CDK6, and PCNA) to accelerate VSMC proliferation, migration, and phenotypic switching, ultimately leading to neointima formation (Fig. 8B). More importantly, the inhibitors of SMYD2 (e.g., LLY-507) and HDAC3 (e.g., RGFP966) have great potential to prevent or alleviate restenosis or reocclusion after PCI or CABG treatment in humans.

## 4. Discussion

The prevention and treatment of coronary restenosis have always been the key to improving the long-term prognosis and quality of life of patients with coronary heart disease. Herein, we demonstrated that targeting both the histone methyltransferase SMYD2 and the deacetylase HDAC3 largely attenuated carotid artery injury-induced neointima formation in mice. In proliferating VSMCs, the SMYD2 expression level was significantly elevated in the nucleus but not in the cytoplasm, and the increased SMYD2 promoted the expression of HDAC3 *via* trimethylation of H3K36; in turn, HDAC3 deacetylated SRF and enhanced its transcriptional activity, thereby promoting VSMC proliferation, migration, and phenotypic switching, and then exacerbating neointima formation. Overall, we identified that the SMYD2–HDAC3–SRF axis is a critical novel pathway involved in neointima formation (Fig. 8B).

SMYD2, a histone methyltransferase, methylates histone H3 at lysine 4 (H3K4) or lysine 36 (H3K36) in the nucleus. These residues serve as binding domains for histone posttranslational modifications and alter chromatin structure to facilitate transcription<sup>36</sup>. Surprisingly, compared with studies showing the regulation of histone methylation by SMYD2, more studies have found that SMYD2 is mainly expressed in the cytoplasm and methylates nonhistone proteins to play a critical role in the regulation of tumor growth<sup>18</sup>. For example, SMYD2 suppresses p53 activity by monomethylation of p53 at Lys370 (p53K370me1), which results in downregulation of p21 and Mdm2 expression and ultimately facilitates cancer cell proliferation<sup>37</sup>. In addition to p53, many nonhistone proteins, such as RB (K810me1 and K860me1), PTEN (K313me1), and ER $\alpha$  (K266me1), can also be monomethylated by SMYD2 in the cytoplasm of cancer cells<sup>18</sup>. In contrast, we found that SMYD2 expression was significantly elevated in the nucleus but not in the cytoplasm of HASMCs in response to proliferative stimulation.

Elevated expression of SMYD2 significantly accelerated VSMC proliferation and neointima formation in mice. Transcriptome sequencing revealed that a large number of SRF target genes were regulated by SMYD2, and SRF overexpression obviously reversed the inhibitory effect of SMYD2 knockdown on VSMC proliferation. Interestingly, SMYD2 neither affected SRF expression nor interacted with SRF but instead enhanced the transcriptional activity of SRF. It has been reported that HDAC3 interacts with MEF2 by directly binding to the MADS-box of MEF2, and the MADS-box is well conserved throughout the MADS superfamily of transcription factors, which includes

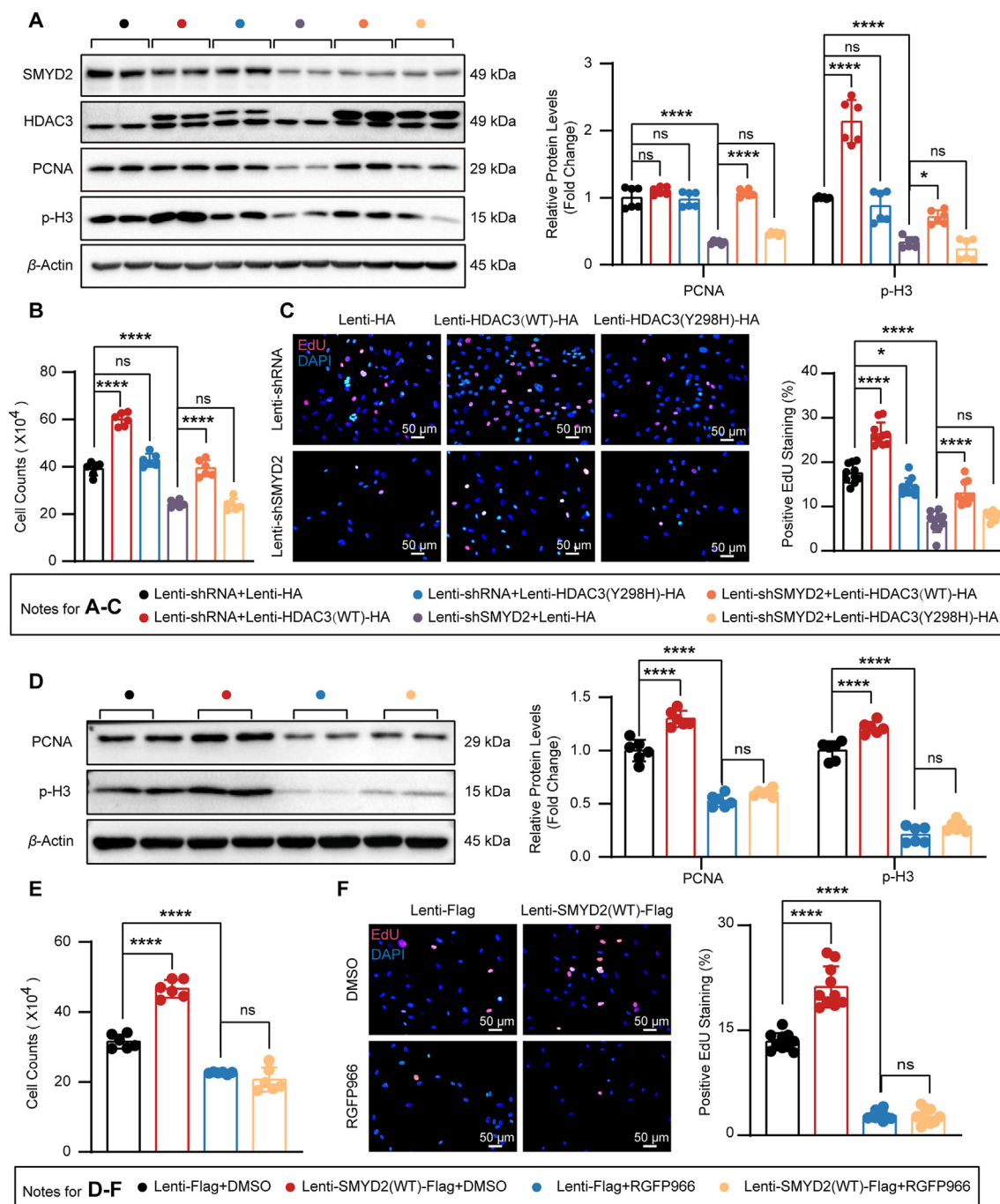


**Figure 7** The deacetylase activity of HDAC3 is required for SMYD2-induced VSMC proliferation. (A) Western blot analysis and quantification showing the protein levels of PCNA and p-H3 in the indicated HASMCs ( $n = 6$ ). SMYD2-silenced HASMCs were infected with lentivirus expressing wild-type HDAC3 or mutated HDAC3 for 48 h, and cell lysates were harvested for western blotting. (B) The counts of HASMCs treated as described in A ( $n = 6$ ). (C) Representative images of immunofluorescence staining and quantification of EdU-positive HASMCs treated as described in A ( $n = 10$ ). (D) Western blot analysis and quantification showing the protein levels of PCNA and p-H3 in the indicated HASMCs ( $n = 6$ ). HASMCs were infected with lentivirus expressing SMYD2 and then treated with RGFP966 for 48 h. (E) The number of HASMCs treated as described in D ( $n = 6$ ). (F) Representative images of immunofluorescence staining and quantification of EdU-positive HASMCs treated as described in D ( $n = 10$ ). The data are presented as the mean  $\pm$  SD, ns indicates no significance; \* $P < 0.05$ ; \*\*\*\* $P < 0.0001$ .

SRF<sup>31</sup>, implying that SRF may interact with HDAC3, and our findings confirm this possibility. HDAC3 is a protein deacetylase, and it has been reported that protein methylation and acetylation often cooperate to regulate many biological processes<sup>38,39</sup>. For example, the histone methyltransferase SETD5 lacks

methyltransferase activity but acts as a scaffold protein in a corepressor complex with HDAC3 and the histone methyltransferase G9a<sup>38</sup>. HDAC3, EZH2 and SOX4 form a complex that binds to the promoter of miR-31 and represses its expression to promote esophageal tumor cell proliferation and invasion<sup>39</sup>. In our

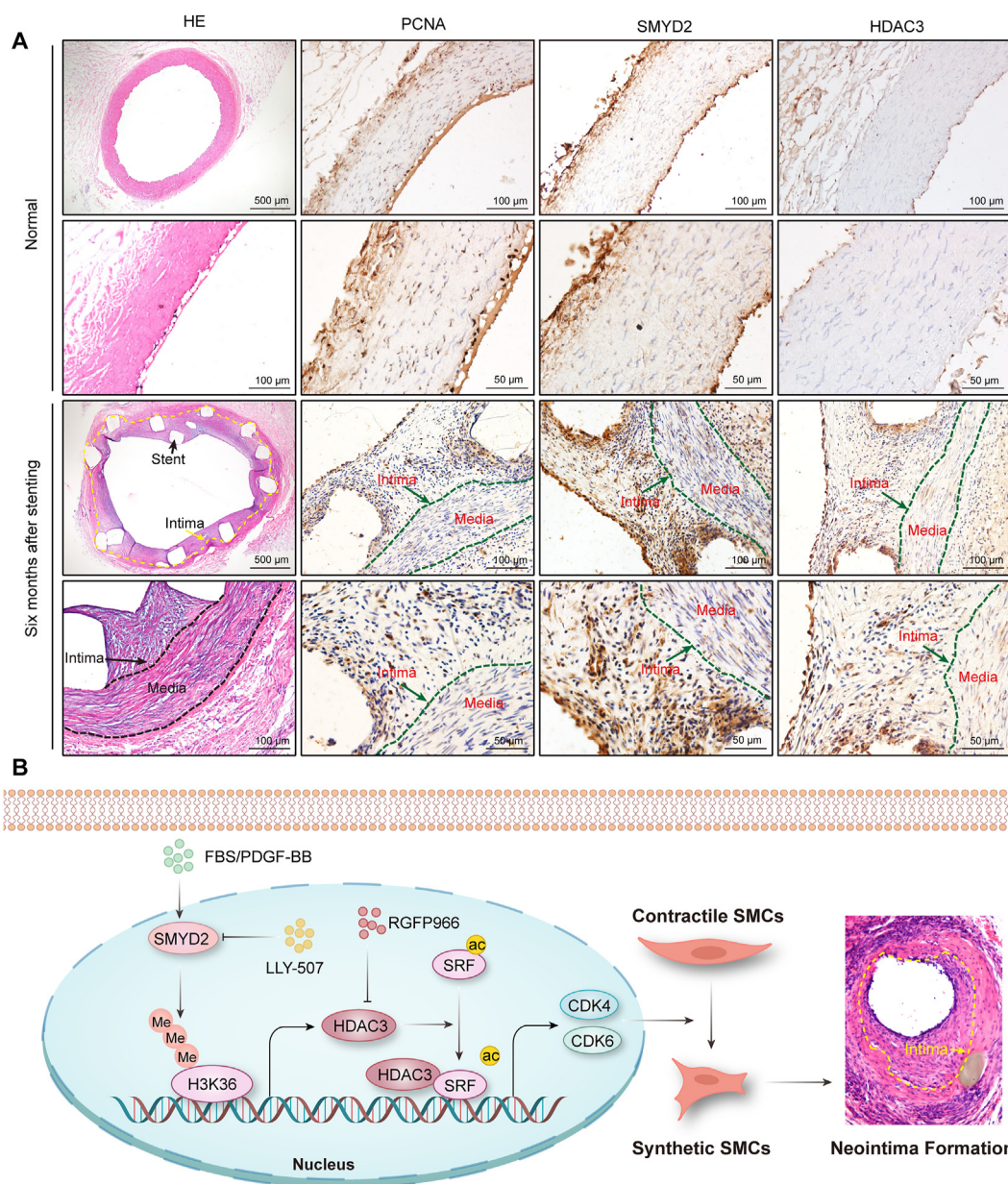


**Figure 8** The SMYD2 and HDAC3 protein abundances are increased in the coronary arteries in a porcine model of post-stent restenosis. (A) Representative images of H&E staining and immunohistochemical staining of PCNA, SMYD2 and HDAC3 in the coronary arteries of pigs with or without post-stent restenosis (scale bar, 50  $\mu$ m, 100  $\mu$ m, 500  $\mu$ m;  $n = 2-5$ ). (B) Schematic showing the mechanism by which the SMYD2-HDAC3-SRF axis modulates neointima formation. FBS or PDGF-BB treatment increases SMYD2 expression following VSMC proliferation, which then promotes HDAC3 transcription by trimethylating H3K36 in the *HDAC3* promoter. HDAC3 interacts with and deacetylates SRF to elevate its transcriptional activity, thereby accelerating VSMC phenotypic switching and neointima formation.

present study, we found that SMYD2 positively regulates the expression of HDAC3 by tri-methylating H3K36 in HASMCs and that RGFP966, a specific inhibitor of HDAC3, obviously alleviates carotid artery injury-induced neointima formation. Moreover, HDAC3 overexpression nullified the effects of SMYD2 knock-down, and RGFP966 offset the impact of SMYD2 overexpression on HASMC proliferation. However, previous studies have shown that HDAC3 performs diametrically opposed functions in endothelial cells<sup>40,41</sup>. HDAC3 has been reported to be involved in maintaining endothelial integrity and supporting atherosclerosis<sup>40</sup>; on the other hand, HDAC3 activation has been found to facilitate the differentiation of Sca-1-positive cells into functional

endothelial cells and accelerate the re-endothelialization of injured arteries<sup>41</sup>. Therefore, further studies are needed to elucidate these seemingly paradoxical functions of HDAC3. Although HDAC3 functions differently in VSMCs and endothelial cells, it mediates the regulation of SMYD2 in VSMCs.

Our aforementioned results confirmed that SRF interacts with HDAC3 and that SRF overexpression largely counteracts the inhibitory effect of RGFP966 on HASMC proliferation. SRF is a transcription factor that can regulate muscle growth and development<sup>42</sup>. SRF directly binds to the SRE in the promoters of its target genes. Previous studies have demonstrated that SRF expression is higher in VSMCs than in other cell types and is associated with

VSMC differentiation<sup>43</sup>. Interestingly, SRF regulates two distinct VSMC gene programs: SMC differentiation genes (SM- $\alpha$ -actin and SMMHC), which are linked to muscle differentiation, and growth-related immediate early genes (IEG and Fos/c-fos), which promote cell growth<sup>44</sup>. Thus, the transcriptional activity of SRF is crucial for the function and phenotype of VSMCs. Since HDAC3 is a deacetylase, we sought to determine whether HDAC3 deacetylates SRF and affects its transcriptional activity. Our results show that HDAC3 inhibitor RGFP966 treatment inhibits SRF deacetylation. Our study shows that in VSMCs, SRF is acetylated, and HDAC3 is involved in regulating the deacetylation of SRF and promoting its transcriptional activity.

It is very common for protein activity to be altered through posttranslational modifications, including acetylation, methylation and phosphorylation. The transcriptional activity of SRF has been reported to be regulated by methylation and phosphorylation<sup>45,46</sup>. For example, methylation of K165 in SRF is required for the transcriptional activation of SRF, which further regulates muscle differentiation; both demethylase KDM2B and methyltransferase SET7 regulate the balance of SRF methylation<sup>47</sup>. Wang et al.<sup>45</sup> found that phosphorylation of SRF enhances the binding of SRF to the VEGFR2 promoter to facilitate its transcription, and GSK-3 was found to phosphorylate and activate SRF to promote axon outgrowth in mouse hippocampal neurons<sup>46</sup>. Phosphorylation of Ser103 in SRF promotes an increase in the width of cardiac myocytes and concentric cardiac hypertrophy through induction of a gene transcription program in concert with activator protein-1 family transcription factors<sup>48</sup>. Our data provide unique insights into the role of SRF deacetylation in the control of VSMC proliferation. Moreover, the deacetylation of SRF is regulated by HDAC3. Although the enzymes that acetylate SRF remain unclear, our results further expand our knowledge of the post-translational modifications of SRF.

In summary, our present work provides both *in vitro* and *in vivo* evidence that the histone methyltransferase SMYD2 functions as a novel positive regulator of VSMC proliferation, migration, phenotypic switching, and neointima formation. The mechanisms underlying the promoting effects of SMYD2 on intimal hyperplasia are associated with direct trimethylation of H3K36, resulting in increased expression of HDAC3, which then deacetylates and activates SRF to accelerate CDK4 and CDK6 transcription (Fig. 8B). More importantly, inhibitors of SMYD2 and HDAC3 have the potential to mitigate neointima formation in mice. We also discovered the acetylation modification of SRF and confirmed that HDAC3 is a deacetylase of SRF. Thus, these observations not only provide new insights into the mechanisms of neointima formation but also could have significant implications for the development of novel strategies to treat restenosis by targeting SMYD2 or HDAC3.

## 5. Conclusions

We found that SMYD2 accelerates VSMC proliferation, migration, phenotypic switching, and neointima formation by promoting HDAC3 expression in a methyltransferase activity-dependent manner. HDAC3 directly interacts with, and deacetylates SRF to facilitate VSMC proliferation and neointima formation. The SMYD2 inhibitor LLY-507 and the HDAC3 inhibitor RGFP966 confer significant protection against vascular injury-induced neointima formation and VSMC proliferation. Thus, the SMYD2–HDAC3–SRF axis is a novel epigenetic mechanism that regulates neointima formation and restenosis.

## Acknowledgments

This work was supported by grants from the National Natural Science Foundation of China (Nos. 81974013 and 82270512).

## Author contributions

Dingsheng Jiang and Xin Yi conceived and supervised the study. Xiaoxuan Zhong and Xiang Wei performed experiments. Yan Xu, Xuehai Zhu, Bo Huo, Xian Guo, Zihao Zhang, Xin Feng, and Zemin Fang contributed to data visualization and performed experiments. Gaoke Feng provided specimens of porcine model of post-stent restenosis. Dingsheng Jiang and Zemin Fang acquired funding. Dingsheng Jiang, Xin Yi, Yuxuan Luo, and Xiaoxuan Zhong wrote the original draft of the manuscript. Dingsheng Jiang, Xin Yi, Yuxuan Luo, and Xiang Wei revised the reviewers' and editorial comments.

## Conflicts of interest

The authors declare no conflicts of interest.

## Appendix A. Supporting information

Supporting data to this article can be found online at <https://doi.org/10.1016/j.apsb.2023.11.012>.

## References

- Jeong K, Kim JH, Murphy JM, Park H, Kim SJ, Rodriguez YAR, et al. Nuclear focal adhesion kinase controls vascular smooth muscle cell proliferation and neointimal hyperplasia through GATA4-mediated Cyclin D1 transcription. *Circ Res* 2019;**125**:152–66.
- Zhang SM, Zhu LH, Chen HZ, Zhang R, Zhang P, Jiang DS, et al. Interferon regulatory factor 9 is critical for neointima formation following vascular injury. *Nat Commun* 2014;**5**:5160.
- Long F, Yang D, Wang J, Wang Q, Ni T, Wei G, et al. SMYD3–PARP16 axis accelerates unfolded protein response and mediates neointima formation. *Acta Pharm Sin B* 2021;**11**:1261–73.
- Fan Y, Chen Y, Zhang J, Yang F, Hu Y, Zhang L, et al. Protective role of RNA helicase dead-box protein 5 in smooth muscle cell proliferation and vascular remodeling. *Circ Res* 2019;**124**:e84–100.
- Torii S, Jinnouchi H, Sakamoto A, Kutyna M, Cornelissen A, Kuntz S, et al. Drug-eluting coronary stents: insights from preclinical and pathology studies. *Nat Rev Cardiol* 2020;**17**:37–51.
- Giacoppo D, Alfonso F, Xu B, Claessen B, Adriaenssens T, Jensen C, et al. Drug-coated balloon angioplasty versus drug-eluting stent implantation in patients with coronary stent restenosis. *J Am Coll Cardiol* 2020;**75**:2664–78.
- Zhang SM, Zhu LH, Li ZZ, Wang PX, Chen HZ, Guan HJ, et al. Interferon regulatory factor 3 protects against adverse neo-intima formation. *Cardiovasc Res* 2014;**102**:469–79.
- McDonald OG, Owens GK. Programming smooth muscle plasticity with chromatin dynamics. *Circ Res* 2007;**100**:1428–41.
- Blackledge NP, Klose RJ. The molecular principles of gene regulation by polycomb repressive complexes. *Nat Rev Mol Cell Biol* 2021;**22**:815–33.
- Zhang M, Urabe G, Little C, Wang B, Kent AM, Huang Y, et al. HDAC6 regulates the MRTF-A/SRF axis and vascular smooth muscle cell plasticity. *JACC Basic Transl Sci* 2018;**3**:782–95.
- Esnault C, Gualdrini F, Horswell S, Kelly G, Stewart A, East P, et al. ERK-induced activation of TCF family of SRF cofactors initiates a chromatin modification cascade associated with transcription. *Mol Cell* 2017;**65**:1081–1095.e5.

12. Chen TQ, Hu N, Huo B, Masau JF, Yi X, Zhong XX, et al. EHMT2/G9a inhibits aortic smooth muscle cell death by suppressing autophagy activation. *Int J Biol Sci* 2020;**16**:1252–63.
13. Li R, Yi X, Wei X, Huo B, Guo X, Cheng C, et al. EZH2 inhibits autophagic cell death of aortic vascular smooth muscle cells to affect aortic dissection. *Cell Death Dis* 2018;**9**:180.
14. Lv Q, Xing Y, Liu J, Dong D, Liu Y, Qiao H, et al. Lonicerin targets EZH2 to alleviate ulcerative colitis by autophagy-mediated NLRP3 inflammasome inactivation. *Acta Pharm Sin B* 2021;**11**:2880–99.
15. Banerji U, van Doorn L, Papadatos-Pastos D, Kristeleit R, Debnam P, Tall M, et al. A phase I pharmacokinetic and pharmacodynamic study of CHR-3996, an oral class I selective histone deacetylase inhibitor in refractory solid tumors. *Clin Cancer Res* 2012;**18**:2687–94.
16. Italiano A, Soria JC, Toulmonde M, Michot JM, Lucchesi C, Varga A, et al. Tazemetostat, an EZH2 inhibitor, in relapsed or refractory B-cell non-Hodgkin lymphoma and advanced solid tumours: a first-in-human, open-label, phase 1 study. *Lancet Oncol* 2018;**19**:649–59.
17. Stein EM, Garcia-Manero G, Rizzieri DA, Tibes R, Berdeja JG, Savona MR, et al. The DOT1L inhibitor pinometostat reduces H3K79 methylation and has modest clinical activity in adult acute leukemia. *Blood* 2018;**131**:2661–9.
18. Yi X, Jiang XJ, Fang ZM. Histone methyltransferase SMYD2: ubiquitous regulator of disease. *Clin Epigenetics* 2019;**11**:112.
19. Jones GT, Tromp G, Kuivaniemi H, Gretarsdottir S, Baas AF, Giusti B, et al. Meta-analysis of genome-wide association studies for abdominal aortic aneurysm identifies four new disease-specific risk loci. *Circ Res* 2017;**120**:341–53.
20. Toghiani BJ, Saratzis A, Freeman PJ, Sylvius N, Bown MJ. SMYD2 promoter DNA methylation is associated with abdominal aortic aneurysm (AAA) and SMYD2 expression in vascular smooth muscle cells. *Clin Epigenetics* 2018;**10**:29.
21. Guo X, Fang ZM, Wei X, Huo B, Yi X, Cheng C, et al. HDAC6 is associated with the formation of aortic dissection in human. *Mol Med* 2019;**25**:10.
22. Feng G, Xiao J, Bi Y, Lan Z, Zheng X, Lu Z, et al. 12-Month coronary angiography, intravascular ultrasound and histology evaluation of a novel fully bioabsorbable poly-L-lactic acid/amorphous calcium phosphate scaffolds in porcine coronary arteries. *J Biomed Nanotechnol* 2016;**12**:743–52.
23. Chen YJ, Li Y, Guo X, Huo B, Chen Y, He Y, et al. Upregulation of IRF9 contributes to pulmonary artery smooth muscle cell proliferation during pulmonary arterial hypertension. *Front Pharmacol* 2021;**12**:773235.
24. Fang ZM, Zhang SM, Luo H, Jiang DS, Huo B, Zhong X, et al. Methyltransferase-like 3 suppresses phenotypic switching of vascular smooth muscle cells by activating autophagosome formation. *Cell Prolif* 2023;**56**:e13386.
25. Munshaw S, Bruche S, Redpath AN, Jones A, Patel J, Dubé KN, et al. Thymosin  $\beta$ 4 protects against aortic aneurysm via endocytic regulation of growth factor signaling. *J Clin Invest* 2021;**131**:e127884.
26. Yuan K, Wang X, Dong H, Min W, Hao H, Yang P. Selective inhibition of CDK4/6: a safe and effective strategy for developing anticancer drugs. *Acta Pharm Sin B* 2021;**11**:30–54.
27. Jia Y, Mao C, Ma Z, Huang J, Li W, Ma X, et al. PHB2 maintains the contractile phenotype of VSMCs by counteracting PKM2 splicing. *Circ Res* 2022;**131**:807–24.
28. Su SC, Hung YJ, Huang CL, Shieh YS, Chien CY, Chiang CF, et al. Cilostazol inhibits hyperglucose-induced vascular smooth muscle cell dysfunction by modulating the RAGE/ERK/NF- $\kappa$ B signaling pathways. *J Biomed Sci* 2019;**26**:68.
29. Brown MA, Sims 3rd RJ, Gottlieb PD, Tucker PW. Identification and characterization of SMYD2: a split SET/MYND domain-containing histone H3 lysine 36-specific methyltransferase that interacts with the Sin3 histone deacetylase complex. *Mol Cancer* 2006;**5**:26.
30. Iram T, Kern F, Kaur A, Myneni S, Morningstar AR, Shin H, et al. Young CSF restores oligodendrogenesis and memory in aged mice via Fgf17. *Nature* 2022;**605**:509–15.
31. Grégoire S, Xiao L, Nie J, Zhang X, Xu M, Li J, et al. Histone deacetylase 3 interacts with and deacetylates myocyte enhancer factor 2. *Mol Cell Biol* 2007;**27**:1280–95.
32. Emmett MJ, Lazar MA. Integrative regulation of physiology by histone deacetylase 3. *Nat Rev Mol Cell Biol* 2019;**20**:102–15.
33. Xu L, Xie H, Hu S, Zhao X, Han M, Liu Q, et al. HDAC3 inhibition improves urinary-concentrating defect in hypokalaemia by promoting AQP2 transcription. *Acta Physiol (Oxf)* 2022;**234**:e13802.
34. Kwapis JL, Alagband Y, López AJ, White AO, Campbell RR, Dang RT, et al. Context and auditory fear are differentially regulated by HDAC3 activity in the lateral and basal subnuclei of the amygdala. *Neuropsychopharmacology* 2017;**42**:1284–94.
35. Xiao J, Feng G, Kang G, Lan Z, Liao T, Kislauskis E, et al. 6-Month follow-up of a novel biodegradable drug-eluting stent composed of poly-L-lactic acid and amorphous calcium phosphate nanoparticles in porcine coronary artery. *J Biomed Nanotechnol* 2015;**11**:1819–25.
36. Yun M, Wu J, Workman JL, Li B. Readers of histone modifications. *Cell Res* 2011;**21**:564–78.
37. Huang J, Perez-Burgos L, Placek BJ, Sengupta R, Richter M, Dorsey JA, et al. Repression of p53 activity by Smyd2-mediated methylation. *Nature* 2006;**444**:629–32.
38. Wang Z, Hausmann S, Lyu R, Li TM, Lofgren SM, Flores NM, et al. SETD5-coordinated chromatin reprogramming regulates adaptive resistance to targeted pancreatic cancer therapy. *Cancer Cell* 2020;**37**:834–49.e13.
39. Koumangoye RB, Andl T, Taubenslag KJ, Zilberman ST, Taylor CJ, Loomans HA, et al. SOX4 interacts with EZH2 and HDAC3 to suppress microRNA-31 in invasive esophageal cancer cells. *Mol Cancer* 2015;**14**:24.
40. Zampetaki A, Zeng L, Margariti A, Xiao Q, Li H, Zhang Z, et al. Histone deacetylase 3 is critical in endothelial survival and atherosclerosis development in response to disturbed flow. *Circulation* 2010;**121**:132–42.
41. Xiao Q, Zeng L, Zhang Z, Margariti A, Ali ZA, Channon KM, et al. Sca-1<sup>+</sup> progenitors derived from embryonic stem cells differentiate into endothelial cells capable of vascular repair after arterial injury. *Arterioscler Thromb Vasc Biol* 2006;**26**:2244–51.
42. Kaplan-Albuquerque N, Van Putten V, Weiser-Evans MC, Nemenoff RA. Depletion of serum response factor by RNA interference mimics the mitogenic effects of platelet derived growth factor-BB in vascular smooth muscle cells. *Circ Res* 2005;**97**:427–33.
43. Miano JM. Role of serum response factor in the pathogenesis of disease. *Lab Invest* 2010;**90**:1274–84.
44. Miano JM. Serum response factor: toggling between disparate programs of gene expression. *J Mol Cell Cardiol* 2003;**35**:577–93.
45. Wang C, Dai X, Wu S, Xu W, Song P, Huang K. FUNDC1-dependent mitochondria-associated endoplasmic reticulum membranes are involved in angiogenesis and neoangiogenesis. *Nat Commun* 2021;**12**:2616.
46. Li CL, Sathyamurthy A, Oldenborg A, Tank D, Ramanan N. SRF phosphorylation by glycogen synthase kinase-3 promotes axon growth in hippocampal neurons. *J Neurosci* 2014;**34**:4027–42.
47. Kwon DH, Kang JY, Joung H, Kim JY, Jeong A, Min HK, et al. SRF is a nonhistone methylation target of KDM2B and SET7 in the regulation of skeletal muscle differentiation. *Exp Mol Med* 2021;**53**:250–63.
48. Li J, Tan Y, Passariello CL, Martinez EC, Kritzer MD, Li X, et al. Signalosome-regulated serum response factor phosphorylation determining myocyte growth in width versus length as a therapeutic target for heart failure. *Circulation* 2020;**142**:2138–54.